GEOS 28600

The science of landscapes:
Earth & Planetary Surface Processes

Lecture 16

Monday 2 March 2020

Chemical weathering processes:

(1) solution

Partial or complete dissolution of a mineral in a solvent; $NaCl \rightarrow Na^{+} + Cl^{-}$

(2) hydration

Hydrolysis: addition of H2O to mineral; $CaSO4 + nH2O \rightarrow CaSO4.nH2O$

(3) hydrolysis

Chemical reaction due to H+ or OH- ions in water; i.e., water is reactant not just a solvent. E.g. albite $NaAlSi_3O_8 + nH_2O \rightarrow Na^{+} + OH^{-} + 2H_4SiO_4 + (1/2)Al_2Si_2O_5(OH)_4$ kaolinite.

(4) chelation

Organic process by which metallic cations are incorporated into hydrocarbon molecules.

(5) oxidation/reduction

e.g. reddening of soils (ferrous → ferric)

(6) carbonation

generation of bicarbonate ion and carbonic acid and its reaction with minerals.

Also: microbially mediated processes; pH due to respiration can be as low as pH 4.5 (this accelerates silicate weathering).

Soil Production Rate (SPR)

Heimsath et al., Nature Geoscience 2012

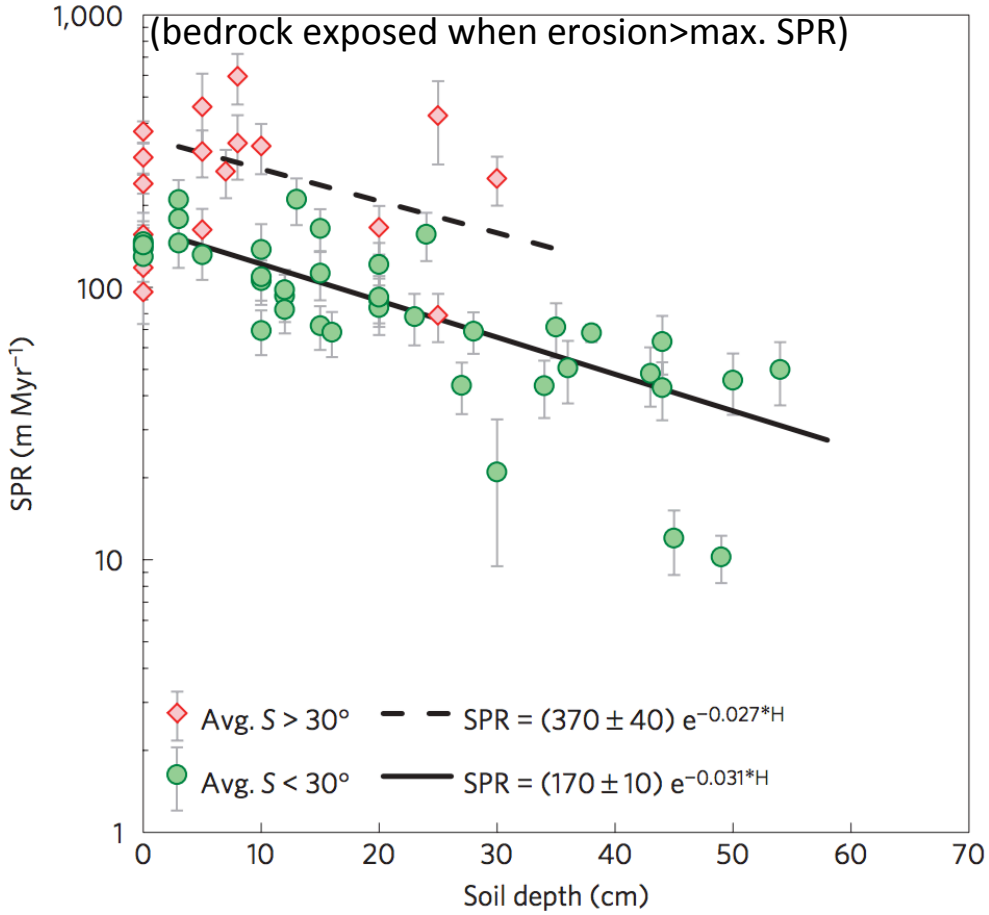

Soil production rates quantified using cosmogenic ^{10}Be (5 atoms/g/yr at sea level)

Earlier "humped" SPR functions now considered dubious

Transport-limited hillslope evolution is well understood; Weathering-limited hillslopes (e.g., Sierra Nevada) not well understood.

but see Larsen et al. Science 2014 for the claim that there is no speed limit on soil production

Fluvial sediment transport vs. hillslope processes: what controls the spacing of rivers?

SETTING THE SPACING OF STREAMS

HILLSLOPE EROSION PROCESSES

SOIL PRODUCTION FUNCTION

SYNTHESIS: PERRON ET AL. 2009

$$\frac{\partial z}{\partial t} = D\nabla^2 z - KA^m\left|\nabla z\right| + U$$

$$\mathrm{Pe} = \frac{KL^{2m+1}}{D}$$

Set Pe = 1, solve for *L*:

$$L_c = \left(\frac{D}{K}\right)^{\frac{1}{2m+1}}$$

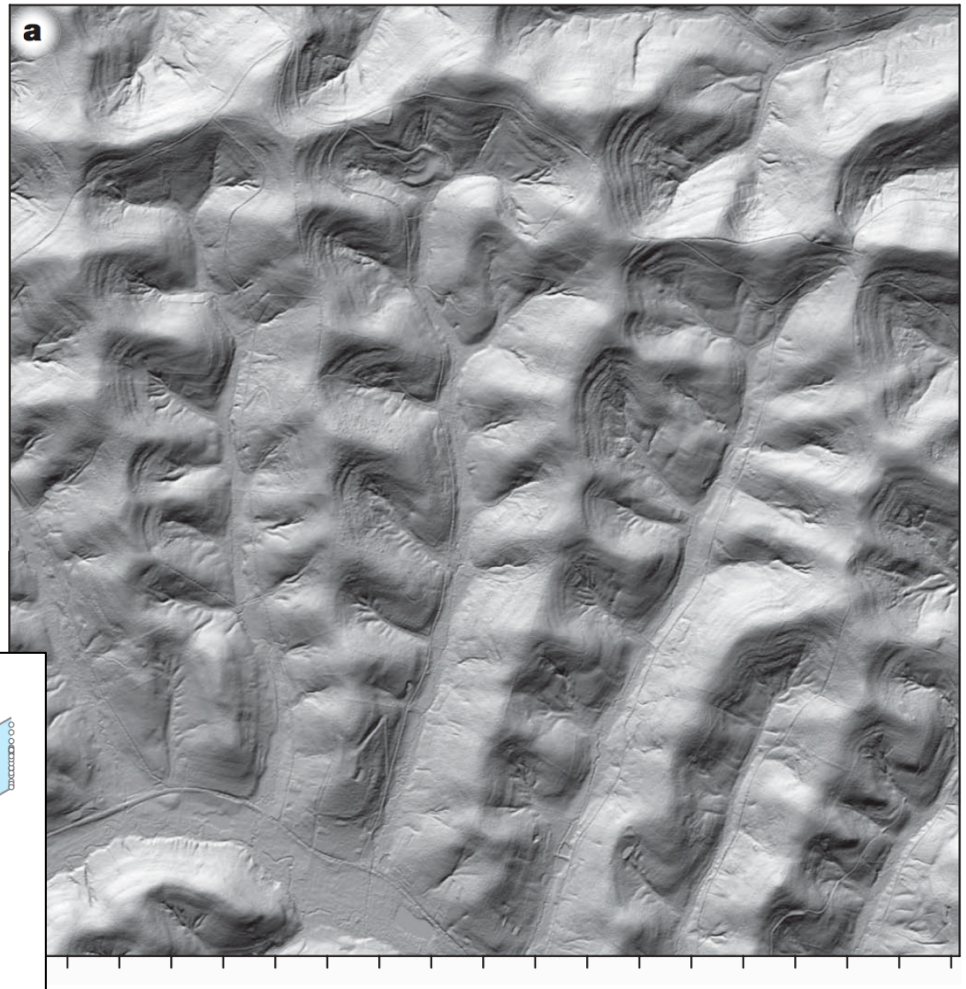

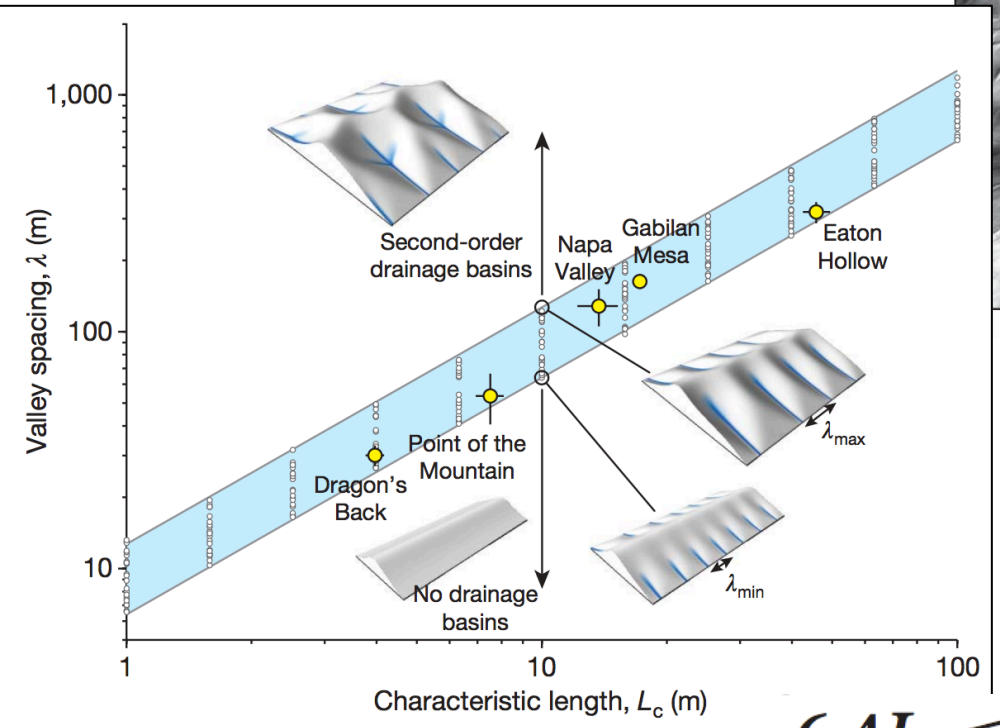

$$6.4L_c \leq \lambda \leq 12.7L_c$$

Key points from today's lecture

- Explain mechanistically how streampower landscapes can act as a tectonic tape-recorder Explain why steady-state hillslopes are convex.
- Explain 2 or more hillslope transport processes.
- Know 2 or more physical and 2 or more chemical weathering processes.
- Understand how Peclet number can quantify competition between hillslope processes and fluvial channelization (see also required reading).

Landscape evolution: sources of data

SOME MAJOR LANDSCAPE EVOLUTION PROBLEMS

DATE/RATE DATA ON EARTH

DATE/RATE DATA ON OTHER PLANETS

In the next lecture, you will be presented dates and rates as facts.
In this lecture, you will be shown the methods that generate these dates and rates: their strengths, weaknesses, and ranges of validity.

Key points

- For each Earth-based dating method, know the principle, advantages, disadvantages, example application, age range of application, for each technique.
- Explain the evidence for and against a Pleistocene uptick in global erosion on Earth (two arguments for and two arguments against, plus geographic context)

Landscape evolution: sources of data

SOME MAJOR LANDSCAPE EVOLUTION PROBLEMS

DATE/RATE DATA ON EARTH

DATE/RATE DATA ON OTHER PLANETS

8 km^3 of sediment were eroded from Earth's continents each year (pre-dam), almost all by fluvial processes, mostly from Asia

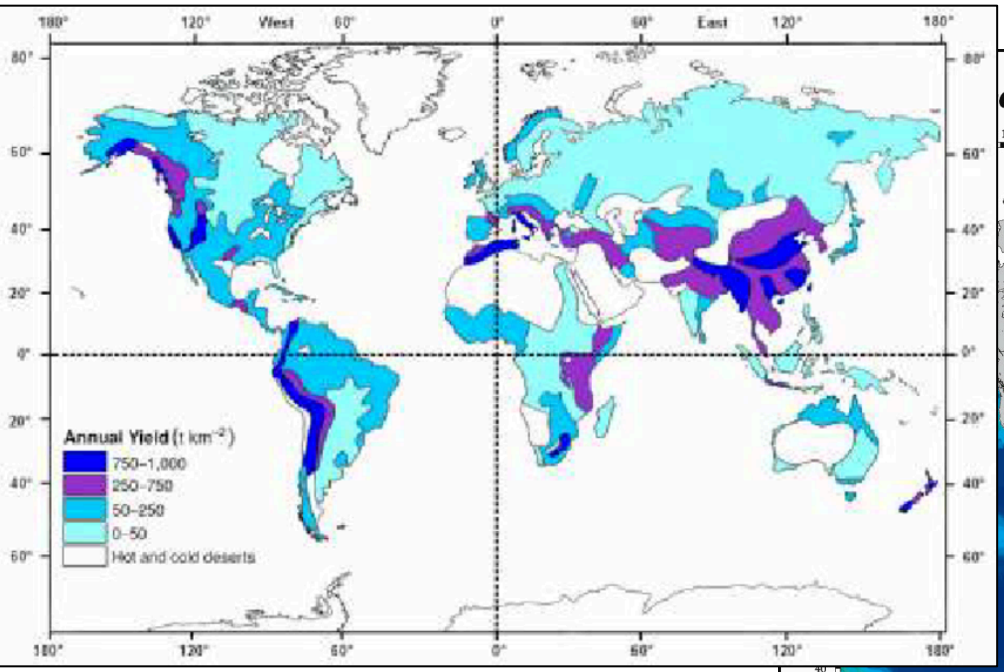

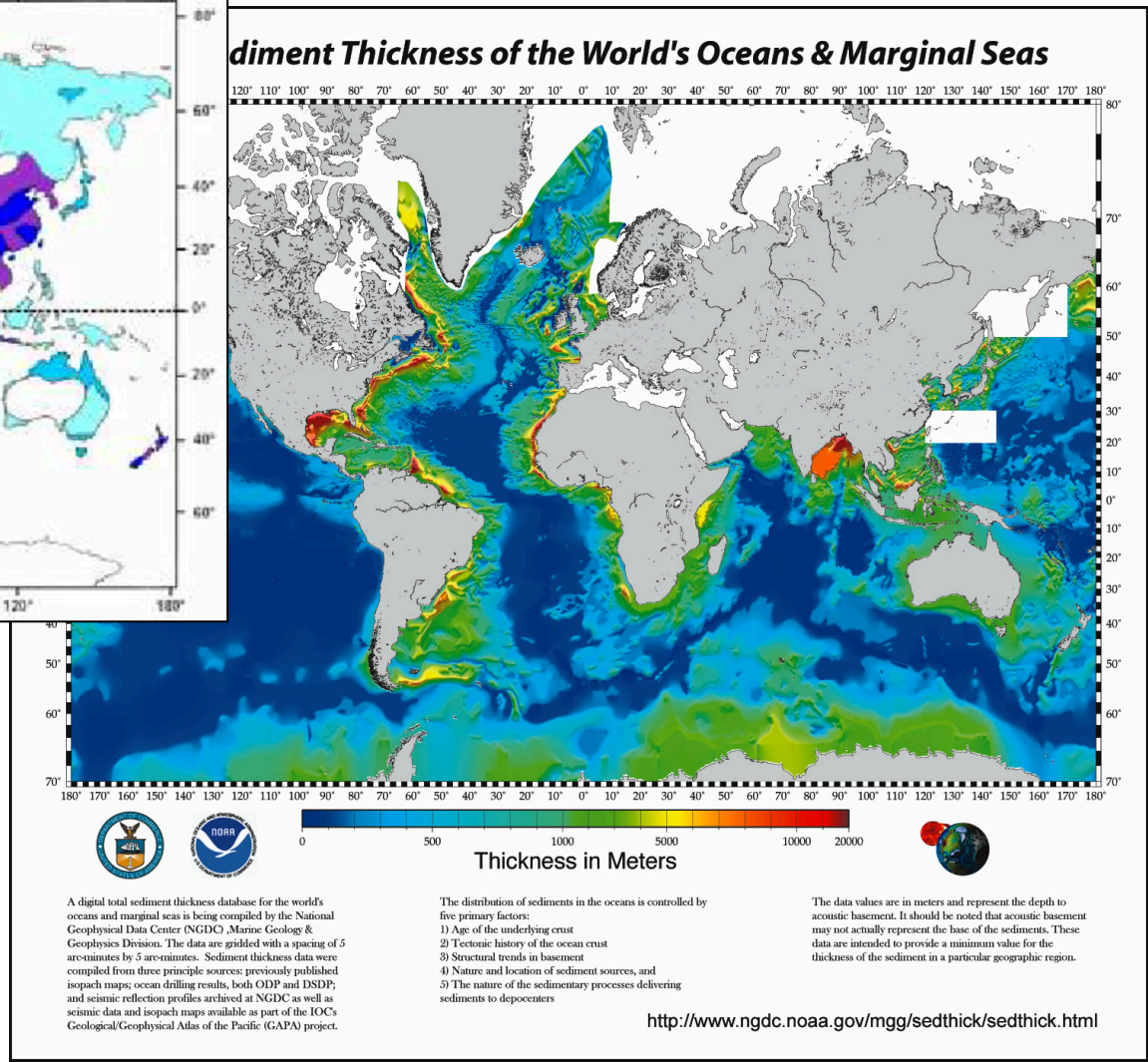

Offshore sediment accumulation rates indicate increase in erosion rates from Asia <2 Mya

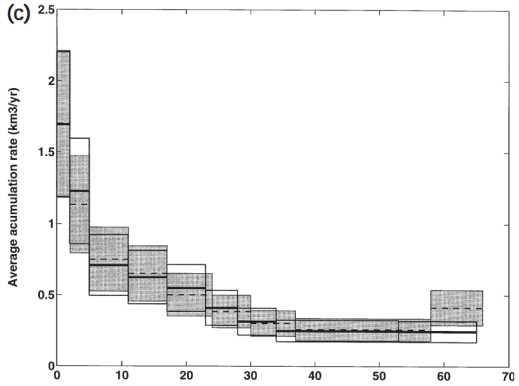

Figure 15. (a) Average SPAR integrated over all basins of Asia. *x*-axis: age in Ma; *y*-axis: rates in $km^3\ yr^{-1}$. Dotted line joining mid-points shows general trend of SPAR. Grey-shaded boxes represent calculation uncertainty. (b) Average fit of SPAR starting from 50 Ma (average age assumed for collision between India and Asia; Patriat & Achache 1984) with an exponential curve. (c) Approximated differences in SPAR induced by use of the Odin (1994) timescale (black lines and empty squares) compared to SPAR obtained using the GSA timescale (Palmer 1983; dotted lines and filled squares).

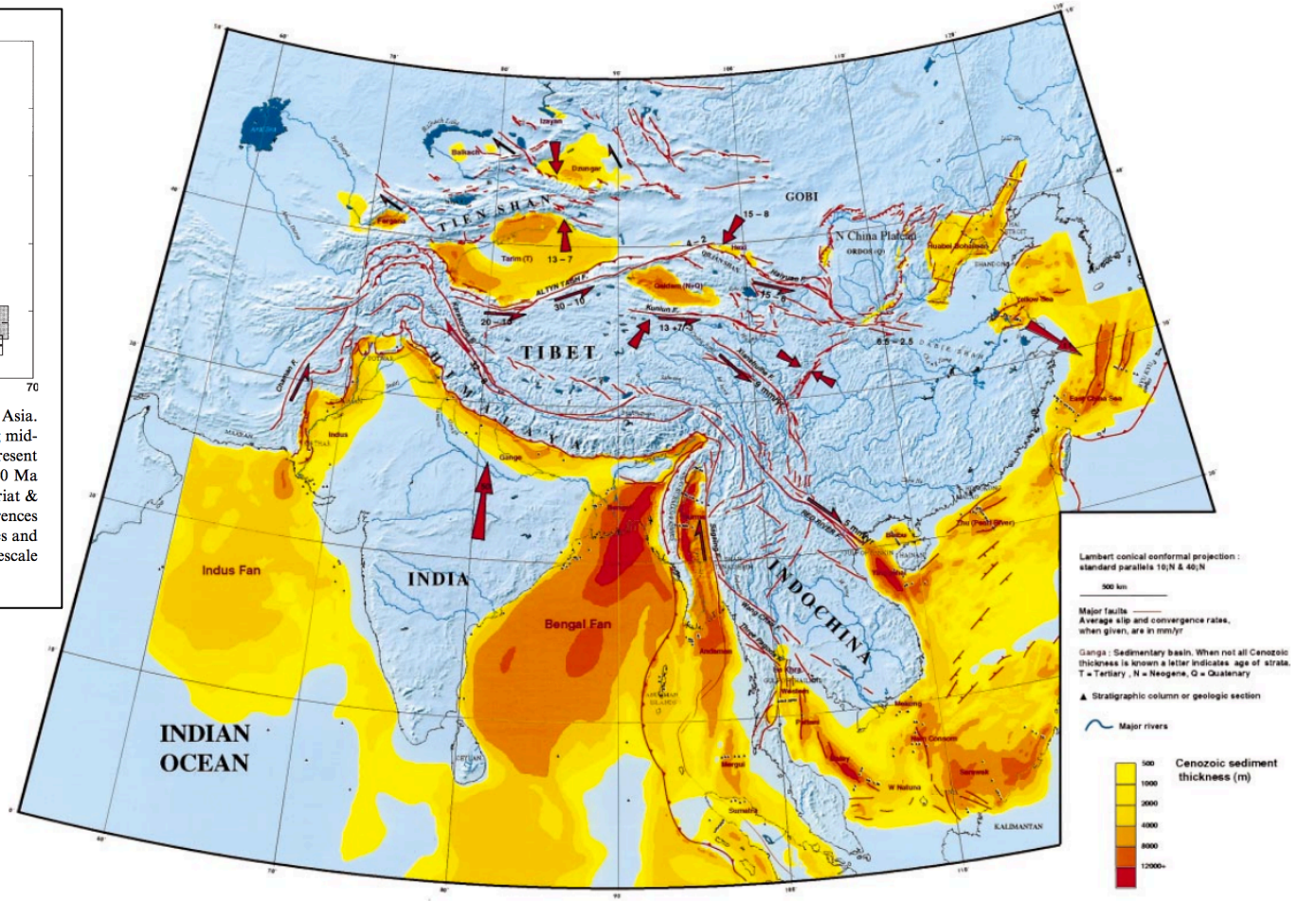

Figure 1. Sedimentary thicknesses in Asia. Maps were digitized and reinterpolated from Sun & Leibo (1984), Vlassov & Diakov (1984), ESCAP (1985), Lee (1985a,b), Rabinowitz *et al.* (1988), Zhu (1990), CCOP (1991) and courtesy of TOTAL CFP. When not otherwise stated sediments are Cenozoic. Hypsography from Defense Mapping Agency (1992). Active faults from Molnar & Tapponnier (1978), Tapponnier & Molnar (1979), Armijo *et al.* (1986, 1989), Tapponnier *et al.* (1986, 1990), Meyer (1991), Avouac *et al.* (1993), Gaudemer *et al.* (1995), Leloup *et al.* (1995) and Lacassin *et al.* (1996). Arrows indicate present-day (India/Siberia, Shanghai) or Holocene rates of displacement and shortening. Small triangles show locations of some of the data used to establish balance.

Metivier et al. 1999 J. Geophys. Int.

This increase has been reported from onshore Asia basins, and globally

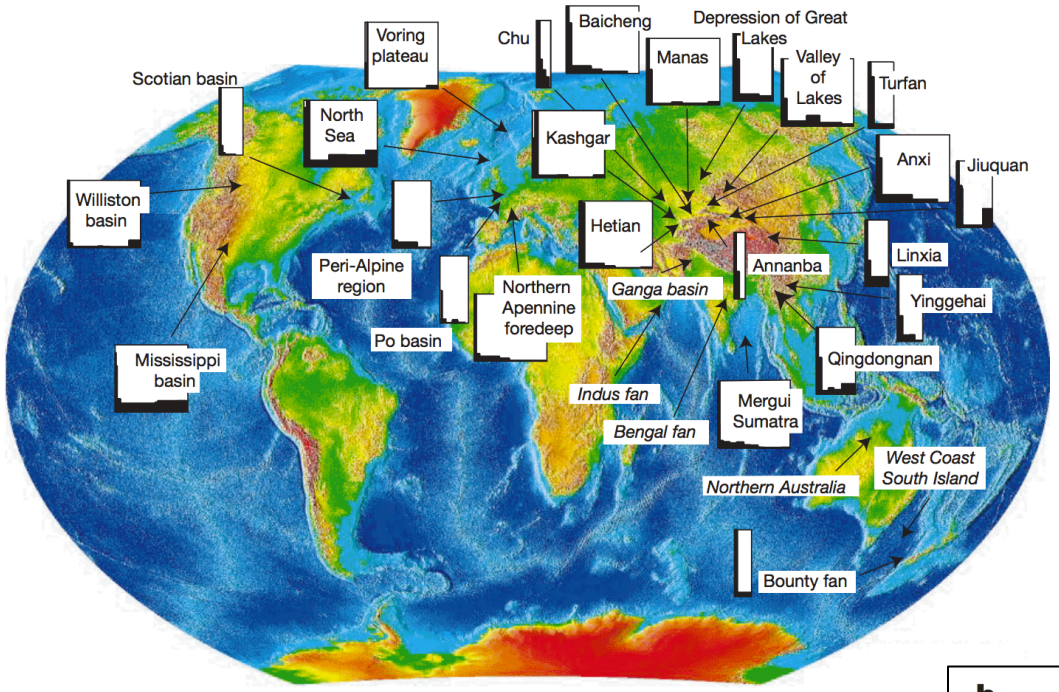

Figure 2 Map of the Earth showing selected areas where sedimentation rates have increased substantially since 2–4 Myr ago. (Details are given in Fig. 4 and Supplementary Information.) For each area, a small histogram is shown. The vertical scale is normalized to the maximum sedimentation rate in that area, and all horizontal ax same timescale; the longest records extend to 65 Myr ago. We sh the Cenozoic for which there are measurements.

Peizhen et al. Nature 2001

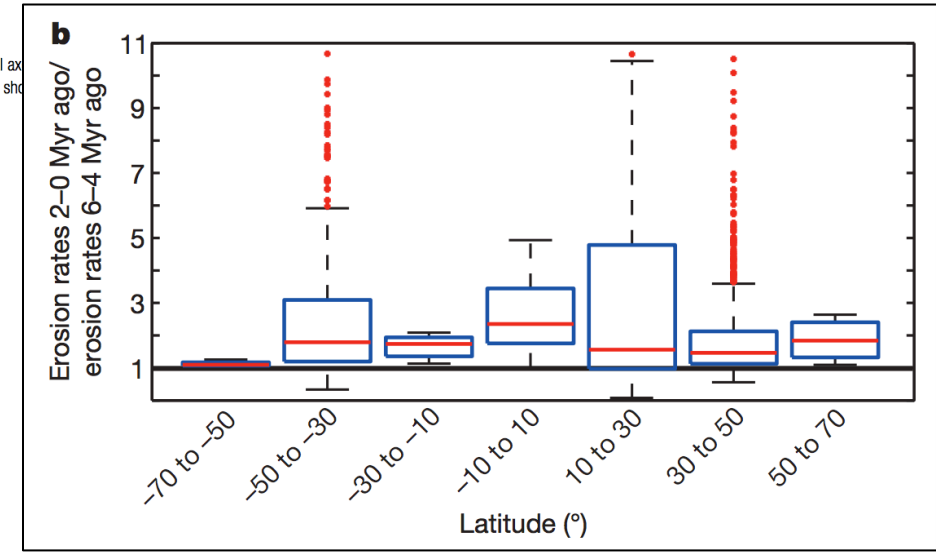

consistent with fission-track data from mountain belts: Herman et al., Nature 2013

However, records of weathering & global tectonics are steady over the last 10 Ma.

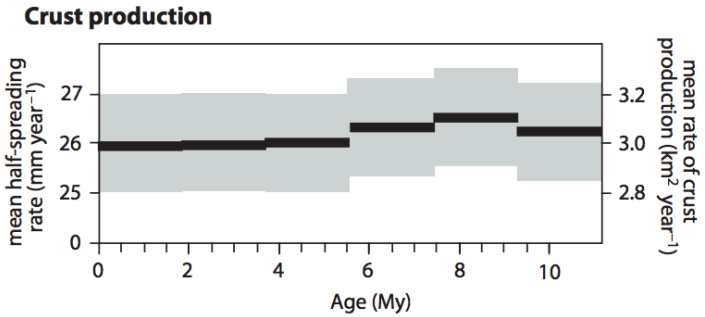

Fig. 1 Rates of tectonic forcing over the last 10 Ma are steady. Figure adapted from Rowley (2002, 2013) and data digitized from Rowley (2002; Fig. 4).

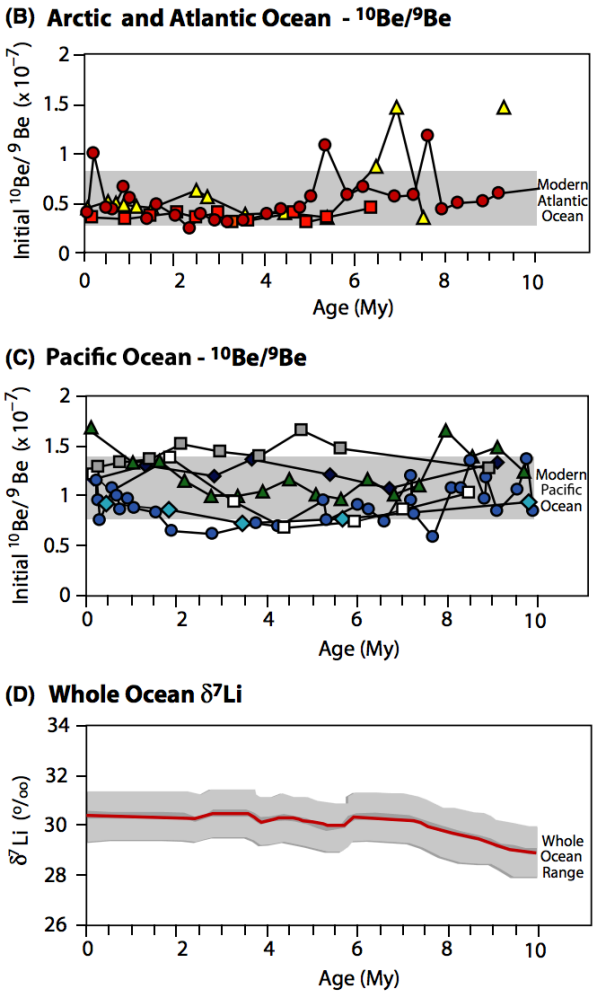

Fig. 2 (A) Palaeo-CO_2 proxy reconstructions from Beerling and Royer (2011) (excluding paleosol proxies) are essentially steady over the last 10 Ma. (B) ^{10}Be/^{9}Be from ferromanganese crusts and dated sediments from the Arctic and Atlantic Oceans (adapted from Willenbring and von Blanckenburg, 2010a). (C) ^{10}Be/^{9}Be from ferromanganese crusts and dated sediments from the Pacific Ocean (adapted from Willenbring and von Blanckenburg, 2010a). Records in (b and c) were corrected for radionuclide decay of ^{10}Be over time and show no systematic variation over the last 10 Ma. (D) Whole ocean δ^7Li records for the last 10 Ma are essentially steady. Figure adapted from Misra and Froelich (2012).

Willenbring & Jerolmack, Terra Nova, 2016

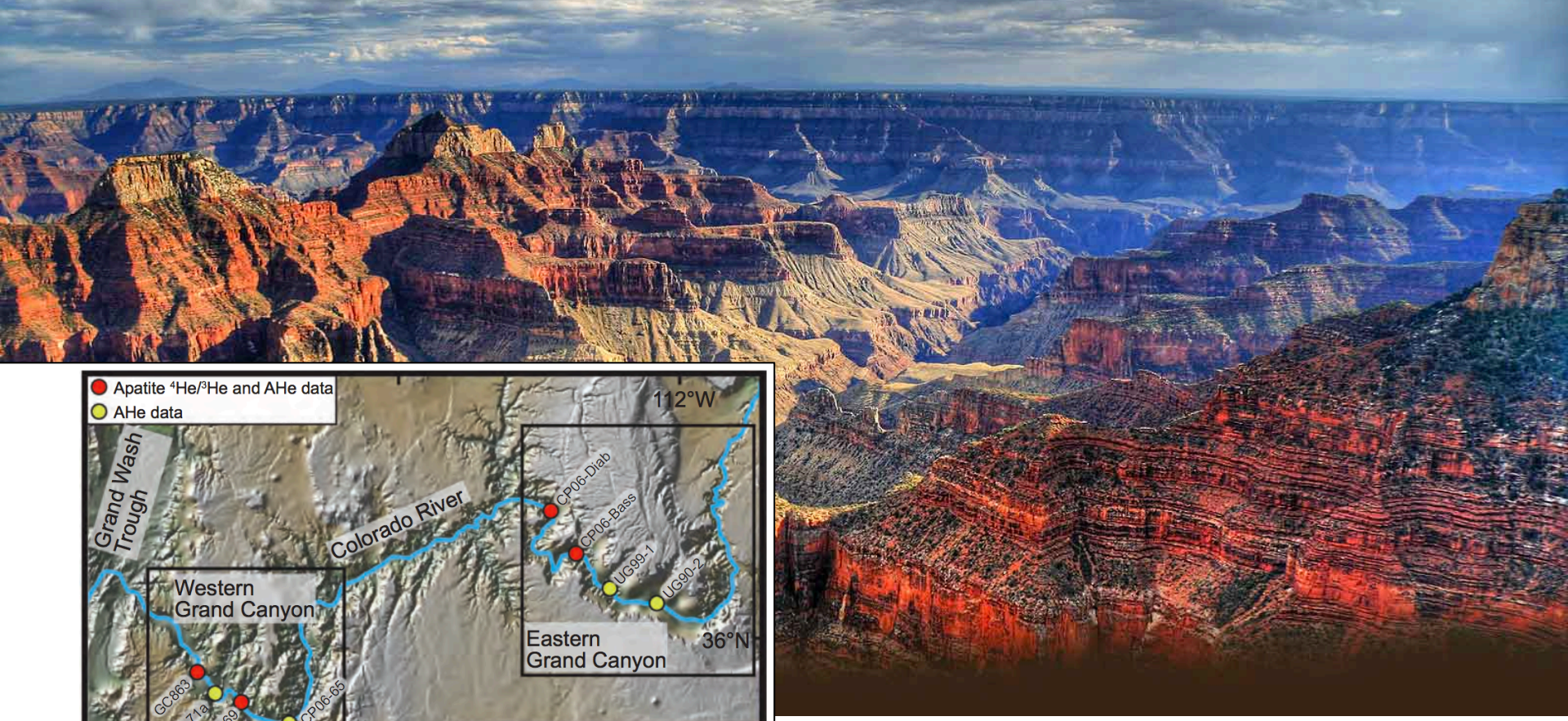

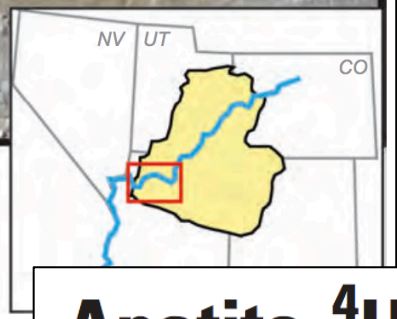

Fig. 1. Grand Canyon shaded relief map showing locations of canyon-bottom samples with apatite $^4He/^3He$ and AHe data simulated in Figs. 2 and 3. The inset marks the location of the study area (red rectangle), the Colorado Plateau (yellow shading), and the Colorado River (blue line) in the southwestern United States.

70 Ma formation of the modern Grand Canyon?

Apatite $^4He/^3He$ and (U-Th)/He Evidence for an Ancient Grand Canyon

R. M. Flowers[1]* and K. A. Farley[2]

Alternative Grand Canyon formation scenario: geologically recent drainage reorganization.

nature geoscience

ARTICLES

PUBLISHED ONLINE: 26 JANUARY 2014 | DOI: 10.1038/NGEO2065

Formation of the Grand Canyon 5 to 6 million years ago through integration of older palaeocanyons

Karl E. Karlstrom[1]*, John P. Lee[2], Shari A. Kelley[3], Ryan S. Crow[1], Laura J. Crossey[1],

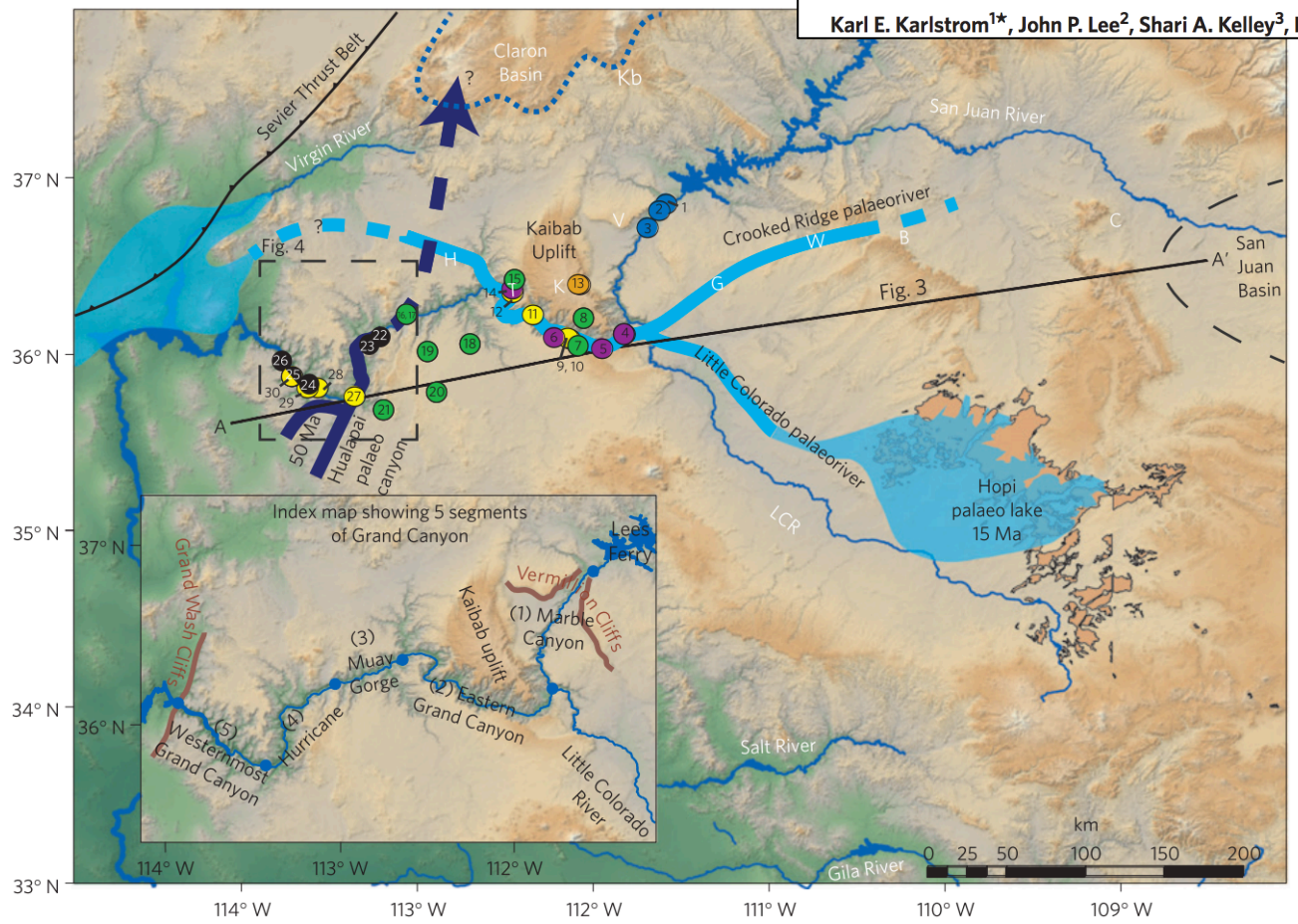

Figure 1 | Map of Grand Canyon. Inset shows segments: (1) Marble Canyon; (2) Eastern Grand Canyon; (3) Muav Gorge; (4) Hurricane fault segment; and (5) Westernmost Grand Canyon. Main map shows inferred drainage at ~15 Ma; B, Black Mesa; C, Chuska Mountains; G, Gap; H, Hack Canyon; K, Kaibab Uplift; Kb, Kaiparowitz Basin; T, Tapeats Creek; V, Vermillion Cliffs; W, White Mesa. Thermochronology samples (Supplementary Table 1): purple, joint AFT and AHE for river-level samples [9]; yellow, river-level samples [2,3]; orange, Kaibab Uplift sample [2,4]; green, rim samples [9]; black, new models. Cross-section line (A–A') for Fig. 3 is shown.

Hindu Fanglomerate, on S rim of W Grand Canyon, 50 Ma, derived from source to Nwards.

Muddy Creek Formation at distal end of Grand Canyon: no deposition before 6 Ma

Landscape evolution: sources of data

SOME MAJOR LANDSCAPE EVOLUTION PROBLEMS

DATE/RATE DATA ON EARTH

DATE/RATE DATA ON OTHER PLANETS

(1) Count layers (tree rings, varves).
(2) Optically stimulated luminescence.
(3) Radiocarbon - ^{14}C.
(4) Spike of radioactive elements (e.g. tritium) associated with atmospheric nuclear testing.
(5) Cosmogenic dating.
(6) Fission track.
(7) (U-Th)/He & other exhumation methods.
(8) Shared event of known age.
(9) The sedimentary record.

(1) Count layers (tree rings, varves)

Varves: annual layers, most commonly in strongly-seasonal lakes

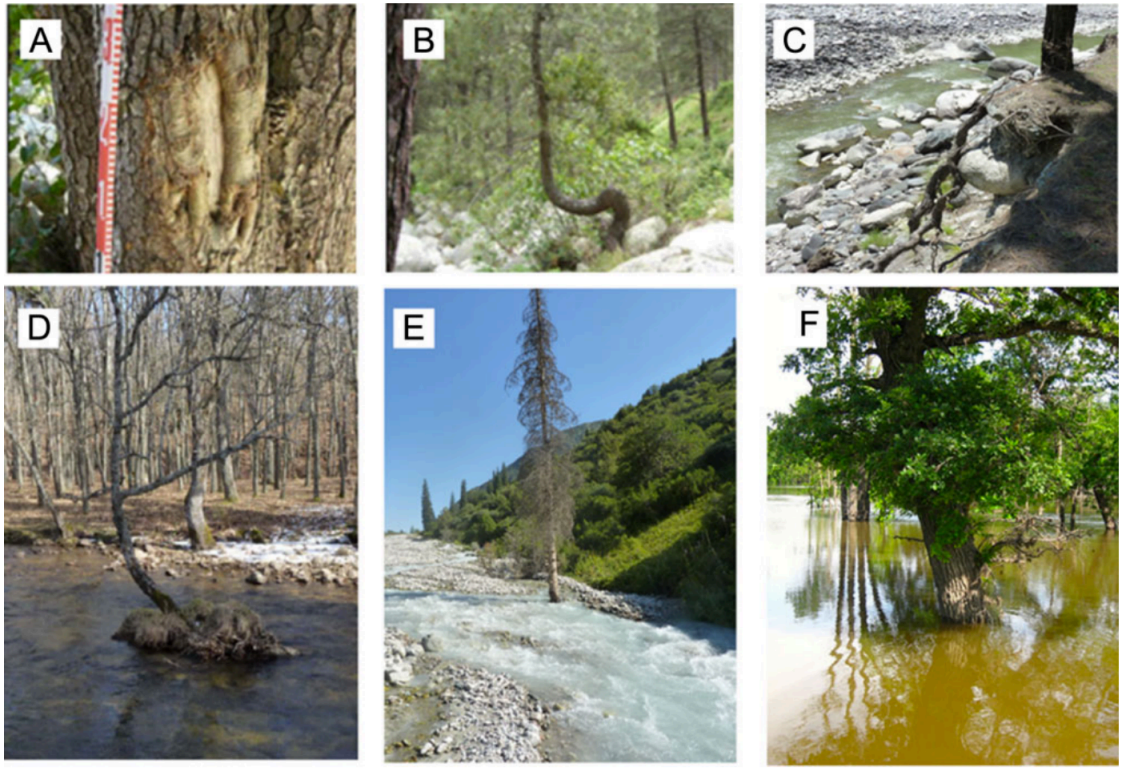

Figure 2. Types of botanical evidence used to identify paleofloods using tree rings. (A) Trees can be injured by the impact or abrasion of boulders or course woody debris transported by flood waters. (B) Flood debris may break the main stem, causing trees do adopt unusual stem morphologies after regrowth. (C) Bank erosion caused by flooding can cause tree roots to become sub-aerially exposed. (D) The hydraulic pressure of floodwaters can tilt tree stems. (E) Changes in channel position or pattern can kill trees growing within the riparian zone. (F) Flooding during the early growing season can cause inundated oak trees to form abnormal anatomical structures within the newly formed wood.

Tree rings – when found embedded in e.g. flood deposits

Ballesteros-Cavenos, Prog. Phys. Geogr. 2015

Example application: mass movements and debris flows → tree death in Southern Alps

Strengths: Well-established, interlocked chronologies for most continents.

Weaknesses: Requires wood preservation (for tree rings). Rarely, tree ring years are “missing” in individual trees.

Time range of application: to 15 Kyr (tree rings); to ~14 Kyr (Cariaco varves); out to 30 Kyr (“floating” varve chronologies, e.g. Lake Suigetsu)

(2) Optically Stimulated Luminescence (OSL)

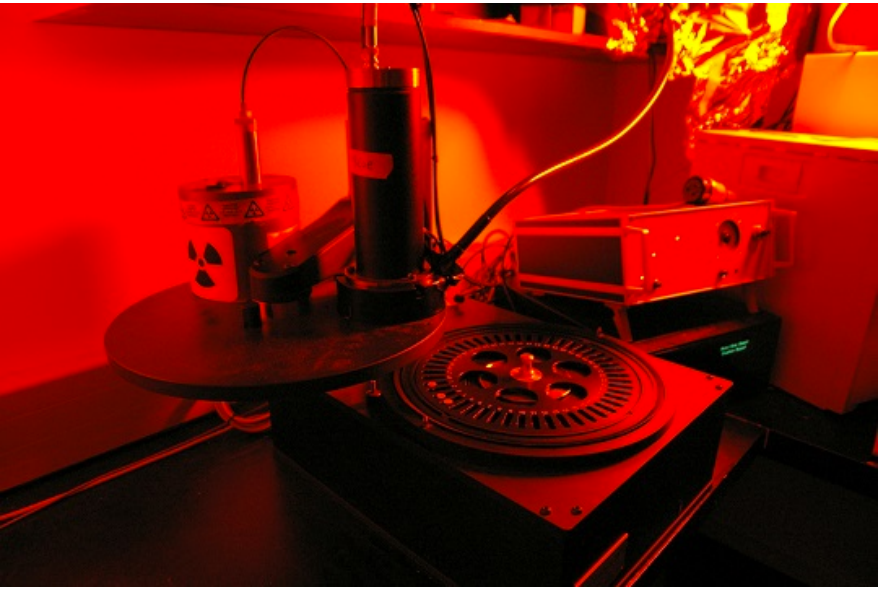

Rhodes et al. Annual Reviews 2011

Strengths: date sand dune overturn, beach sands …

Weaknesses: 5-10% uncertainty; usually requires quartz; collection can be difficult (age reset by 1s of light).

Age range of validity: 0.1-350 Kyr with quartz (out to 1 Myr with feldspar)

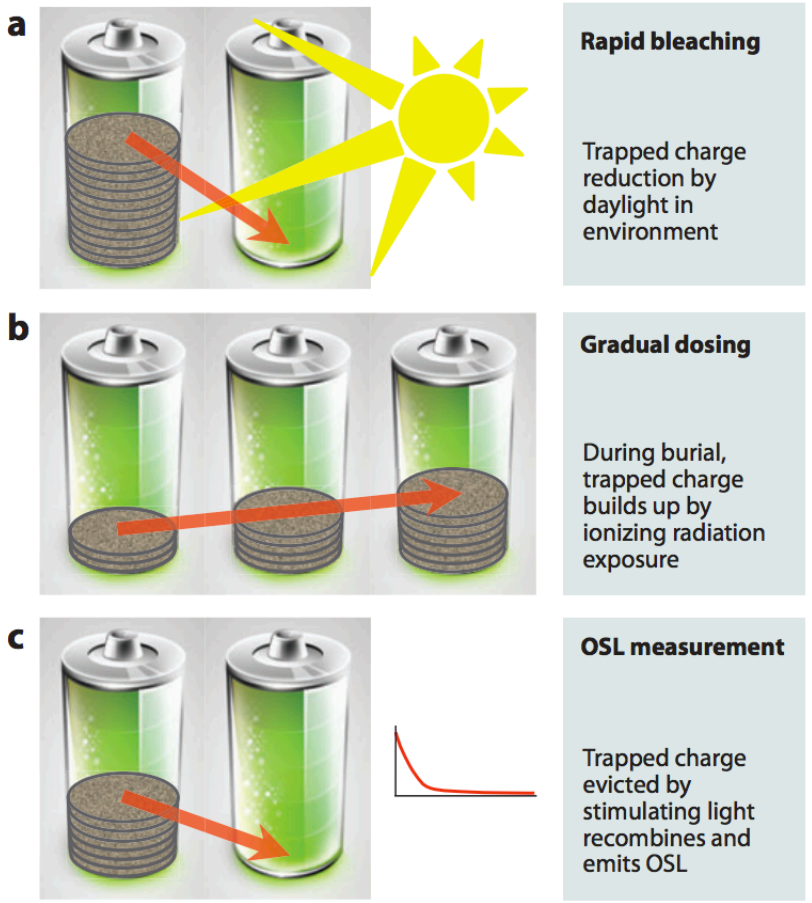

Figure 4

The rechargeable battery forms a useful analogy to help understand optically stimulated luminescence (OSL) dating; gray circles show charge level. (*a*) Daylight releases trapped charge during grain movement over periods of seconds to minutes. (*b*) Charge is slowly built up as a small fraction of electron-hole pairs produced by low levels of environmental radiation are trapped at defects. (*c*) After sample collection and preparation, intense stimulating light releases charge from light-sensitive traps, which recombines emitting UV luminescence, in the form of an OSL decay (shown). Based on an illustration by Duller (2008).

Mechanism of OSL:

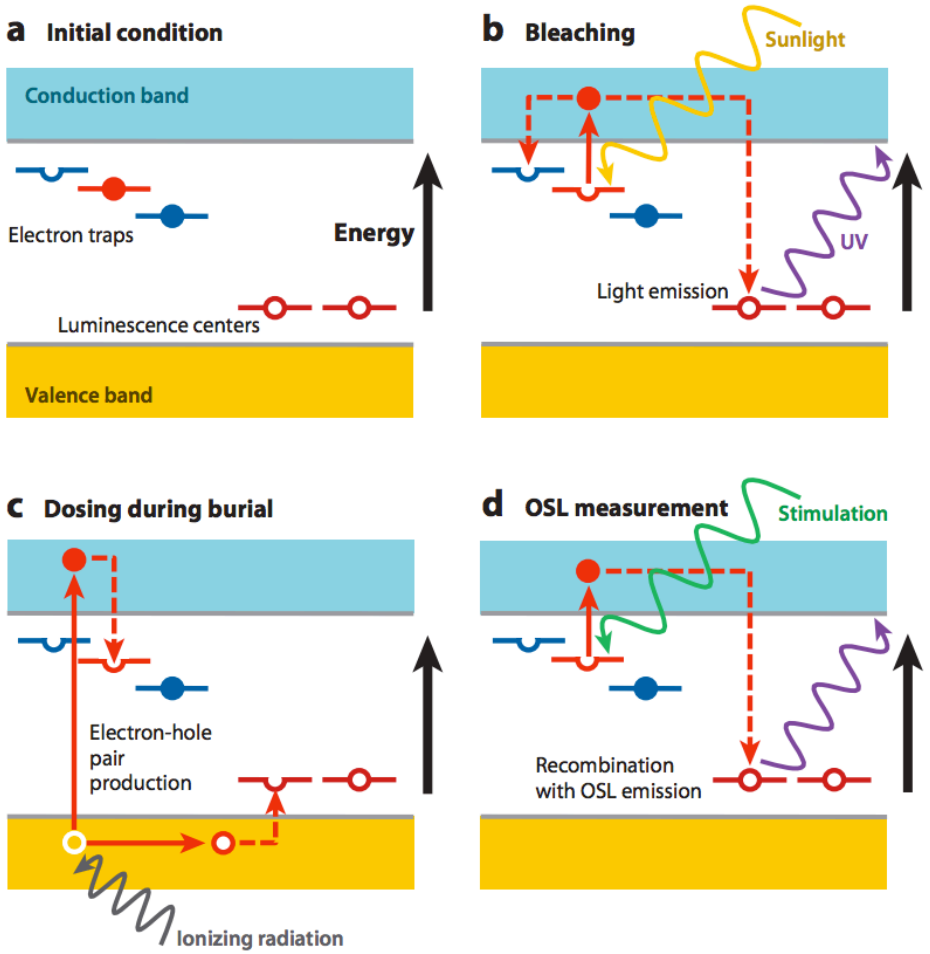

Figure 2

Simple band gap energy model of optically stimulated luminescence (OSL). Light-sensitive (OSL) electron traps are shown in red, light-insensitive (thermoluminescence) traps in blue. (*a*) Under typical initial conditions, low thermal stability traps close to the conduction band are kept empty by thermal eviction at ambient temperature, but other traps are filled; luminescence centers are available. (*b*) On light exposure, electrons in OSL traps are evicted and may become trapped in other available trapping sites or may recombine at hole centers (luminescence centers). After brief light exposure, all OSL traps are emptied. (*c*) During subsequent burial, ionizing radiation gradually produces electron-hole pairs, some of which may become trapped, increasing the OSL trap population. (*d*) Following collection and mineral separation, intense blue-green stimulating light is directed at the sample. Electrons are evicted from OSL traps and recombine at luminescence centers, emitting UV luminescence, detected through glass filters with a photomultiplier tube. As the remaining OSL trap populations falls, the emission rapidly decays to a low level.

(3) Radiocarbon - ^{14}C.

Atmosphere contains ^{14}C (half-life 6 Kyr) due to cosmic-ray bombardment
Plants/soil organisms take up ^{14}C from atmosphere and isolate it upon burial
Isolation date can be constrained by measuring present-day ^{14}C concentration.

$$\frac{N_o}{2} = N_o e^{-\lambda t_{1/2}}$$
$$\frac{1}{2} = e^{-\lambda t_{1/2}} \qquad (6.5)$$
$$t_{1/2} = -\frac{1}{\lambda}\ln\left[\frac{1}{2}\right]$$

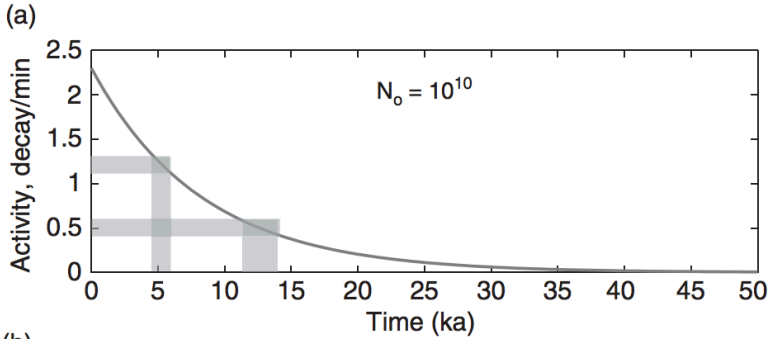

New method: Accelerator Mass Spectroscopy
Eliminates molecular isobars (e.g. ^{13}CH) by accelerating sample to >>KeV and passing through a thin graphite foil.

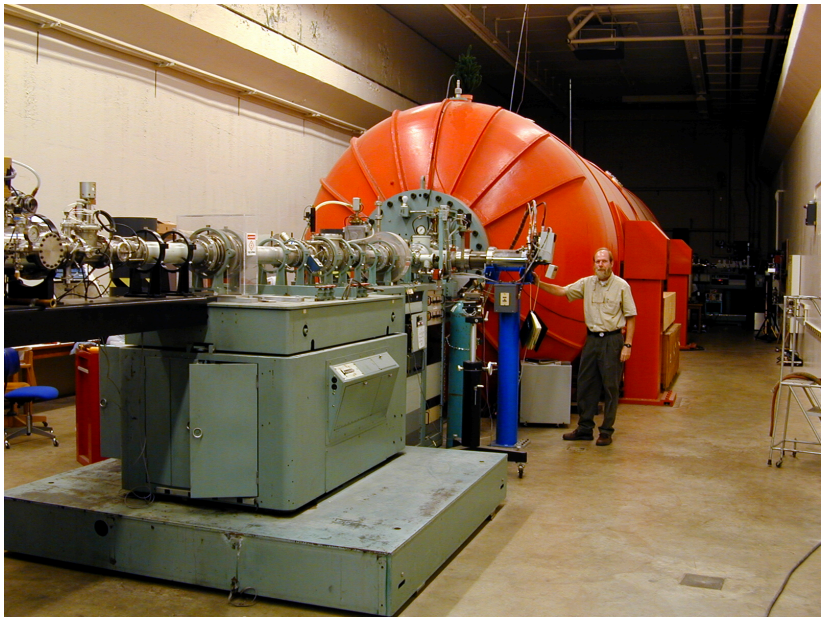

Mark Chaffee (Purdue)

Strengths: Precise, widely used,
can date soil profiles & fluvial deposits.
Example weaknesses: Reworking of old wood, decay of ancient organic matter.
Time range of validity: 50+ Kyr

^{14}C measurements are very precise, but are affected by several systematic biases. "^{14}C age" is not equal to actual age. Ages are reported this way to allow for future improvements in ^{14}C de-biasing.

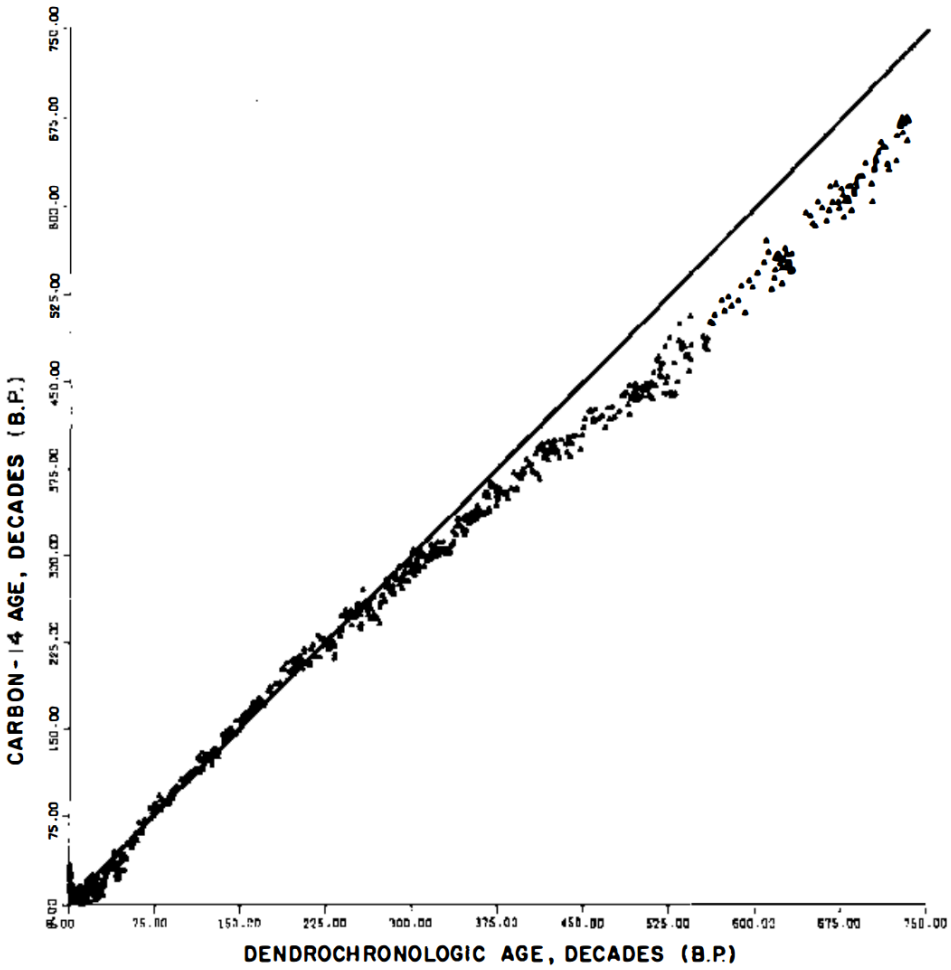

Past atmosphere contained more radiocarbon

Damon et al. Annual Reviews 1978

^{14}C uncertainty is affected by variations in the rate of production (& atmospheric content) of ^{14}C.

Varying magnetic field on Earth:

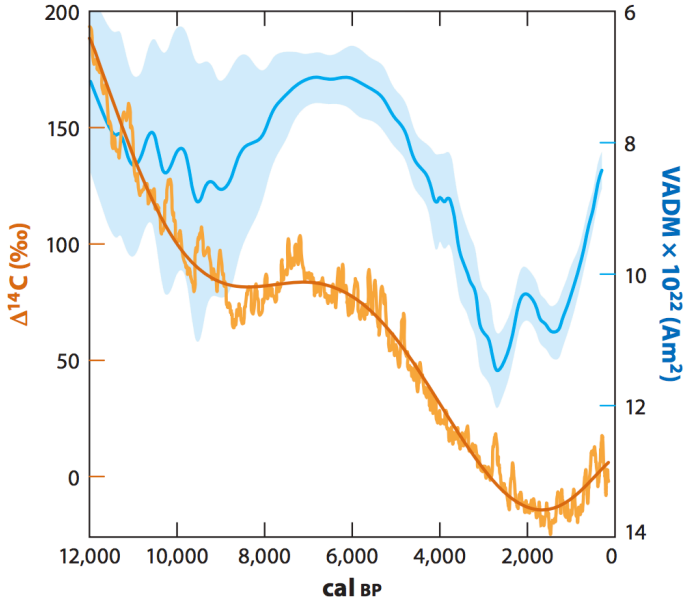

VADM = Virtual Axial Dipole Moment
(Strength of Earth's magnetic field)

Varying solar activity (De Vries effect):

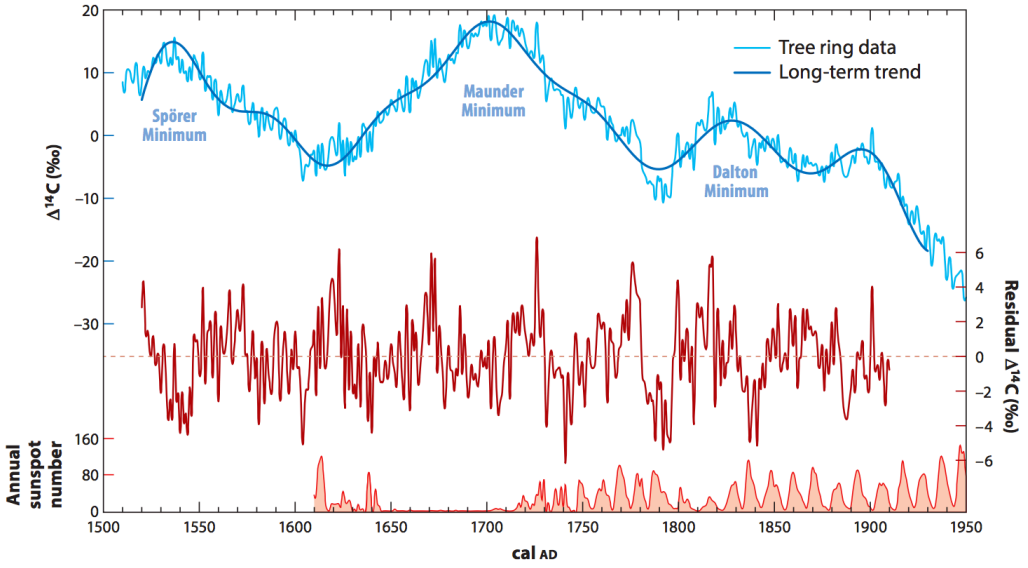

Figure 7

University of Washington Single Year (UWSY; Stuiver & Braziunas 1993b) $\Delta^{14}C$ data in tree rings from the Pacific Northwest (*thin light blue line*) showing the long-term trend (*thick dark blue line*). Periods of major minima (Spörer, Maunder, and Dalton) of solar activities over the last five centuries correspond to higher levels of atmospheric $\Delta^{14}C$. The addition of fossil fuel CO_2 after the onset of the Industrial Revolution lowered levels of atmospheric $\Delta^{14}C$ between 1900 and 1950. The middle curve (*dark red*) represents residuals of $\Delta^{14}C$, obtained by subtracting the long-term trend from the single-year data. The annual sunspot numbers observed since AD 1610 are indicated by the filled red curve at the bottom.

Also: Varying rates of atmosphere-ocean exchange.

(4) Spike of radioactive elements (e.g. tritium) associated with atmospheric nuclear testing

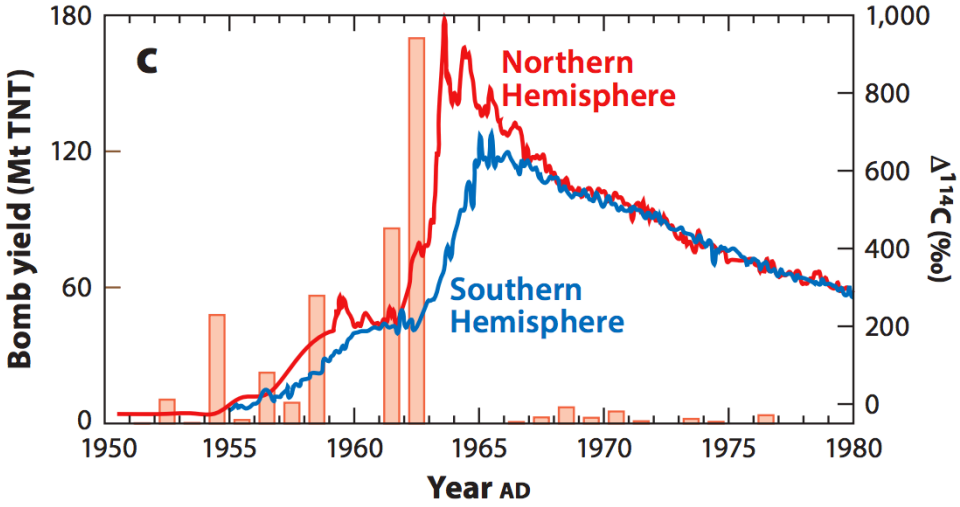

Also: fossil-fuel burning dilutes atmopsheric C with radioactively-inert C

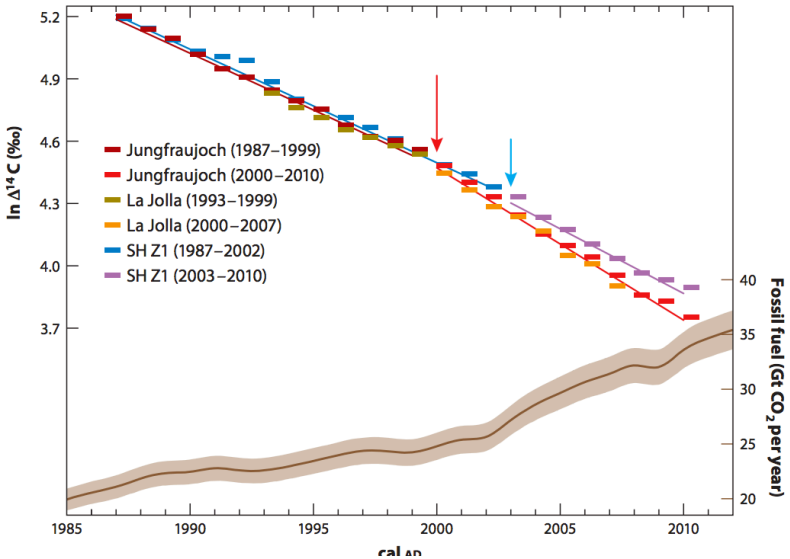

Dutta, Annual Reviews, 2016

(5) Cosmogenic dating

Alongside LIDAR, one of the two most important innovations in geomorphology in the last 20 years

- Produced within rock (not absorbed from atm.), mostly by neutrons
- 10Be, 26Al, 36Cl are radioactive
- Depth profiles allow correction for inheritance

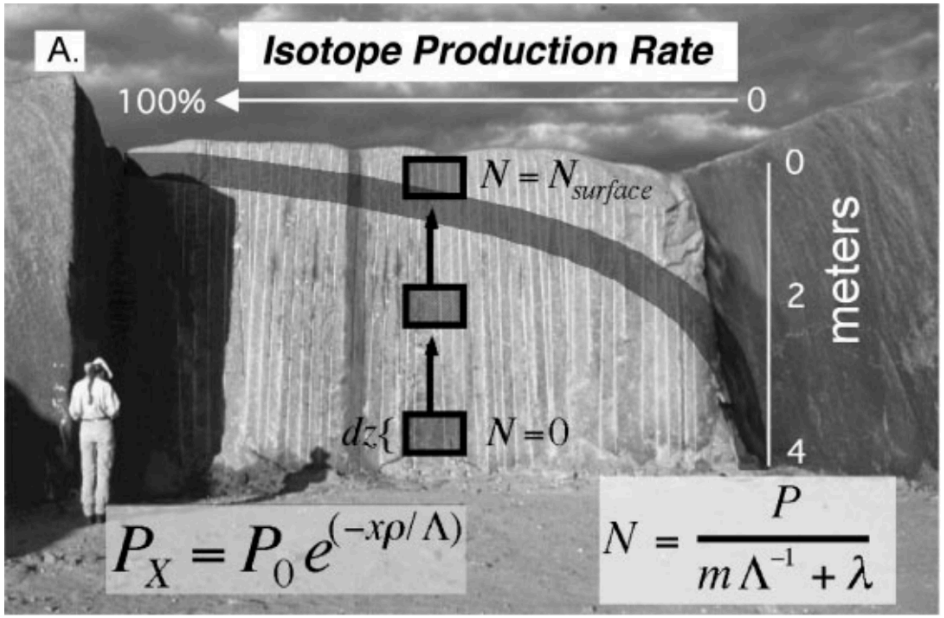

Bierman & Nichols Annual Reviews 2004

Anderson & Anderson, ch. 6

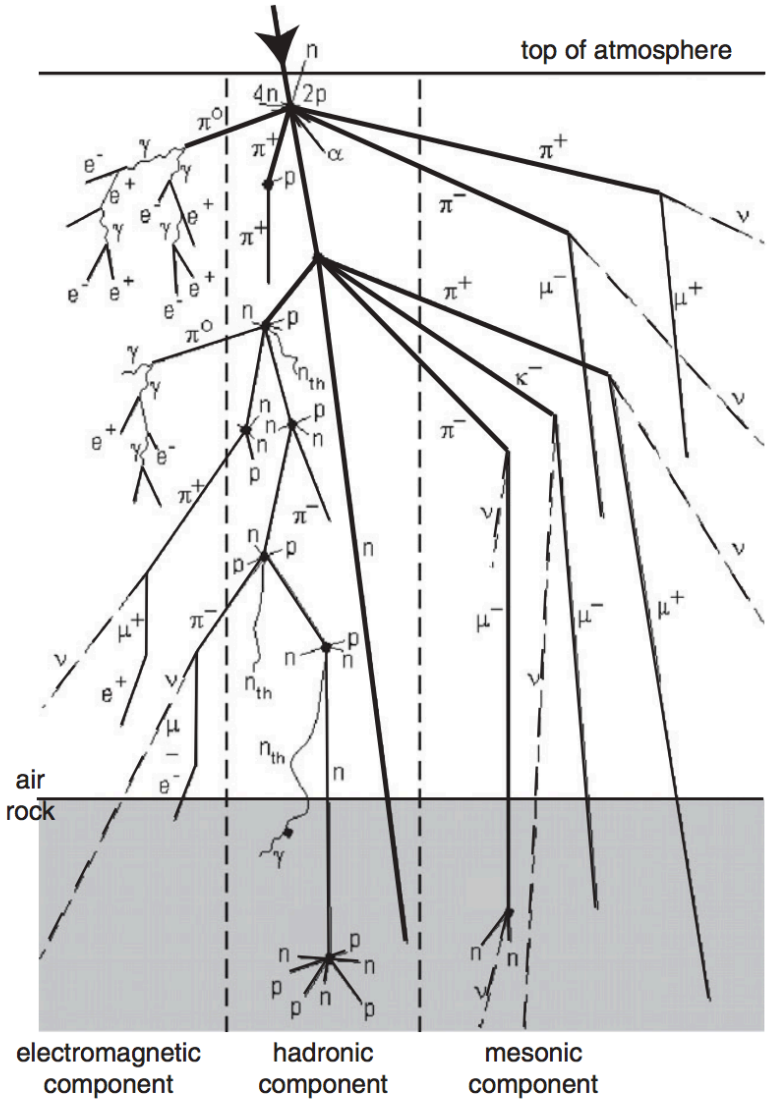

Figure 6.12 Cascade of particle interactions generated by the entrance of a high-energy particle at the top of the atmosphere. Cosmogenic nuclides produced both in the atmosphere and in the top few meters of rock most commonly result from at least secondary particles.

Equilibrium between production and decay for cosmogenic radionuclides with no erosion

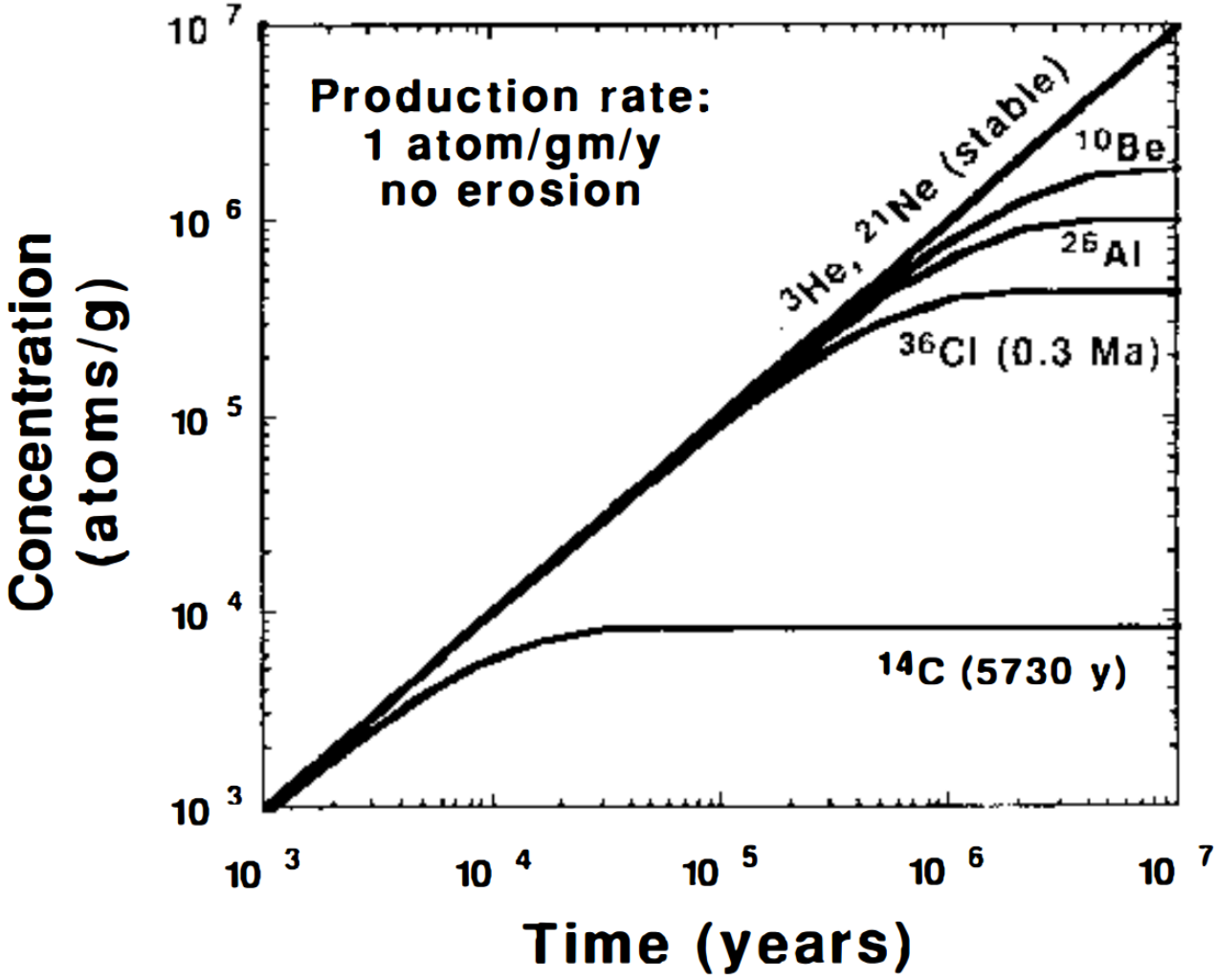

Figure 8 Concentration of in-situ cosmogenic isotopes for a sample with a constant production rate for the case with no erosion. Radioactive cosmogenic isotopes approach a steady-state concentration after about 5 half-lives.

Equilibrium between production and erosion for a stable cosmogenic isotope (e.g., 3He)

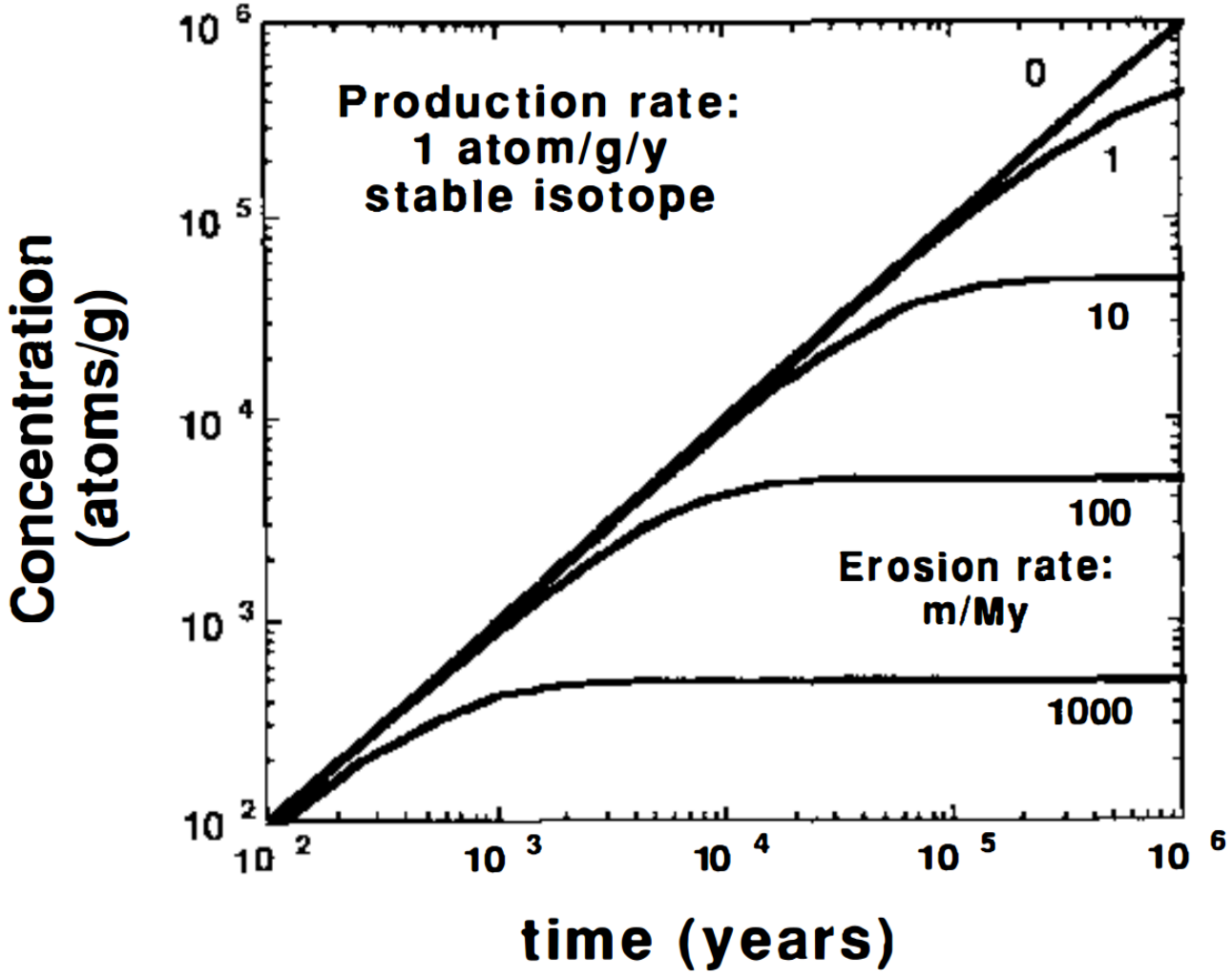

Figure 9 Concentrations of in-situ stable isotopes for samples with erosion rates ranging from 0 to 1000 m/My.

Softer cosmic ray energy spectrum
at high latitudes (due to Earth's magnetic field)

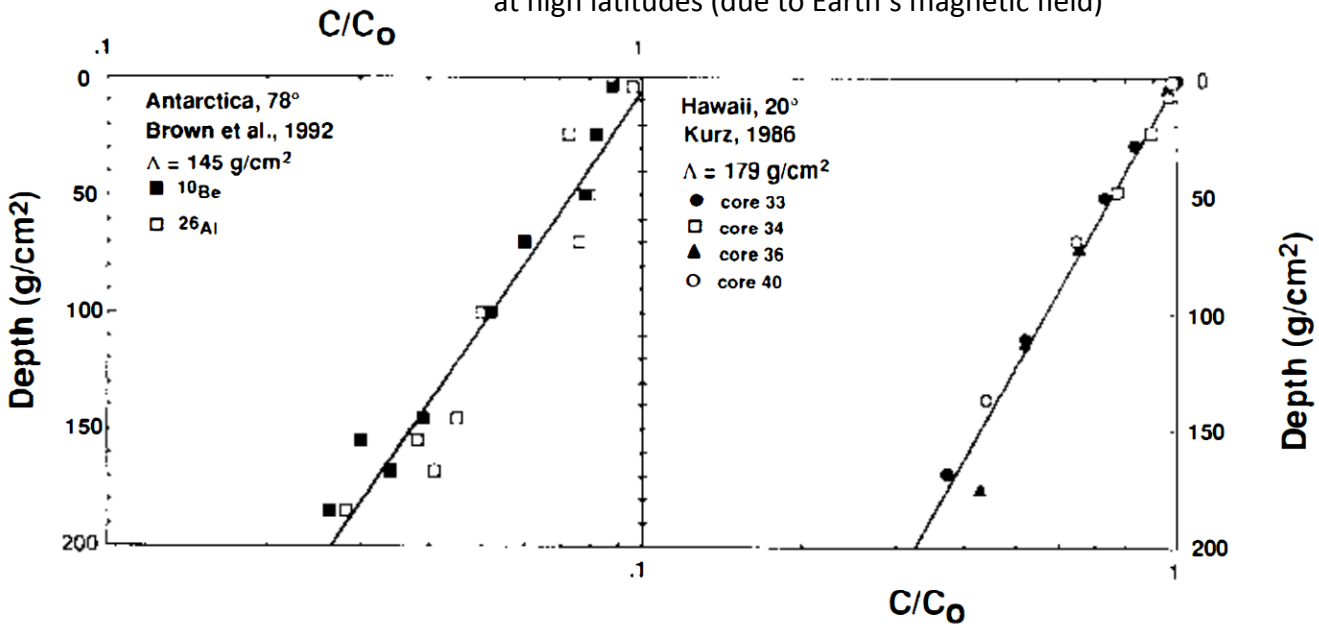

Figure 2 Mass attenuation effects for samples from high latitude and from low latitude. Data from Brown et al (1992) and Kurz (1986b) for rock sample depths less than 200 g/cm^2. Concentrations are normalized to the Earth's surface.

Cerling & Craig,
Annual Reviews 1994

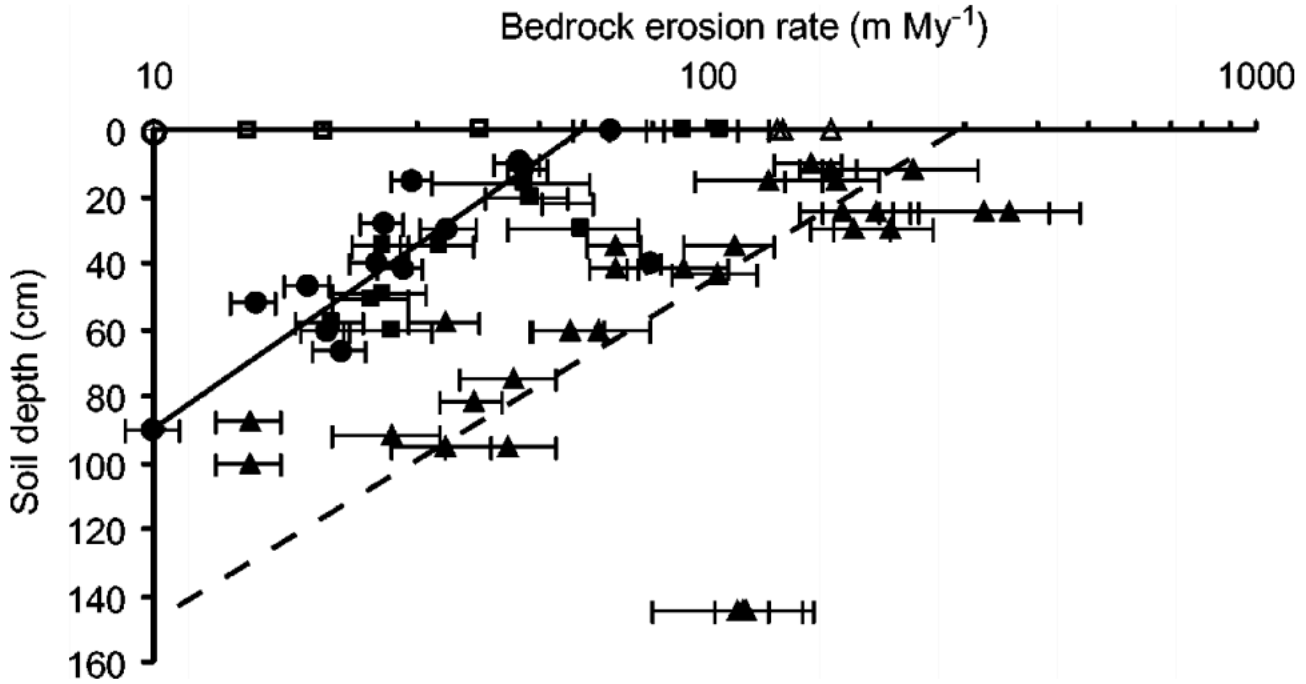

Figure 12 Compilation of soil production rates versus soil depth showing that bedrock erosion rates decrease as soil cover depth increases. Exposed outcrop samples are shown as open symbols and soil production rates are shown as filled symbols for southeastern Australia (*circles*); for Tennessee Valley, California (*squares*); and for Sullivan Creek, Oregon (*triangles*). Modified from Heimsath et al. (1997, 2000, 2001).

Bierman et al. Annual Reviews 2012

(6) Fission track dating

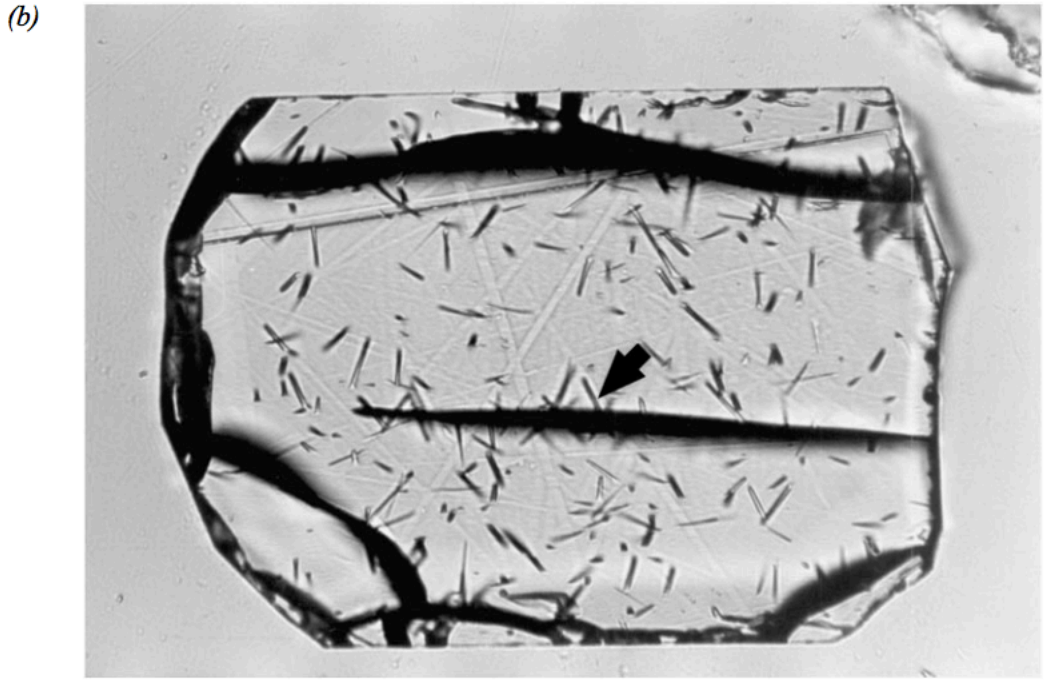

Figure 2 (*a*) Transmission electron microscope images of an unetched fission track in fluorapatite (from Paul & Fitzgerald 1992; reproduced with permission from the Mineralogical Society of America). (*b*) Photomicrograph of a polished and etched prismatic section through an apatite crystal, showing etched surface intersecting tracks and a horizontal confined track (*arrow*). The acid etchant reached the confined track through a large fracture. The long axis of the grain is ~150 μm.

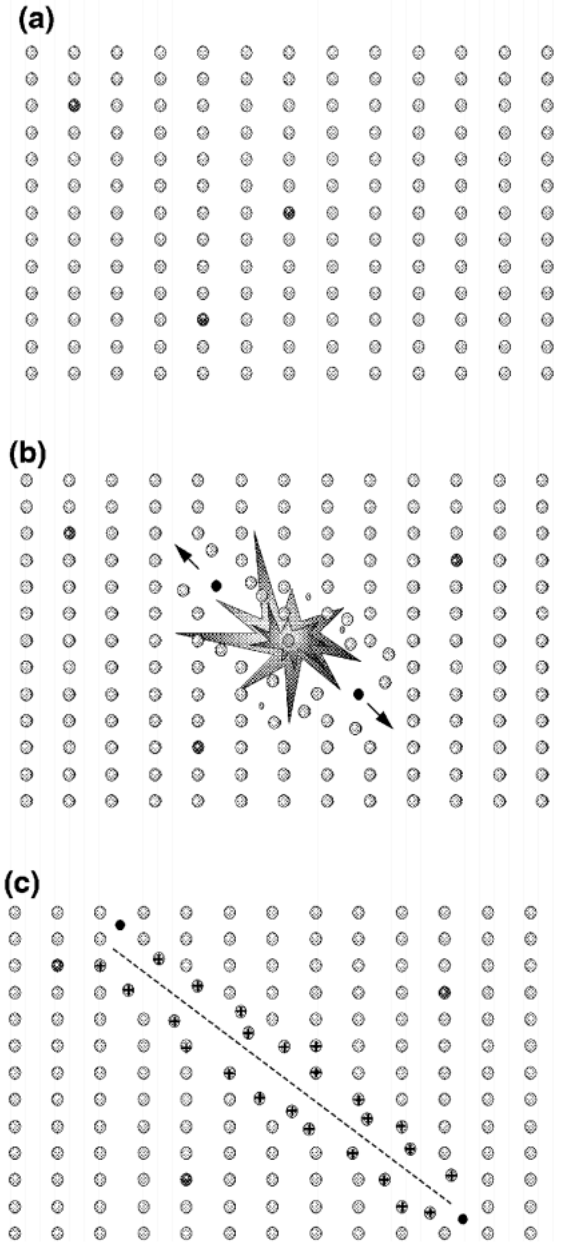

Gallagher et al. Annual Reviews 1998

The meaning of "closure temperature"

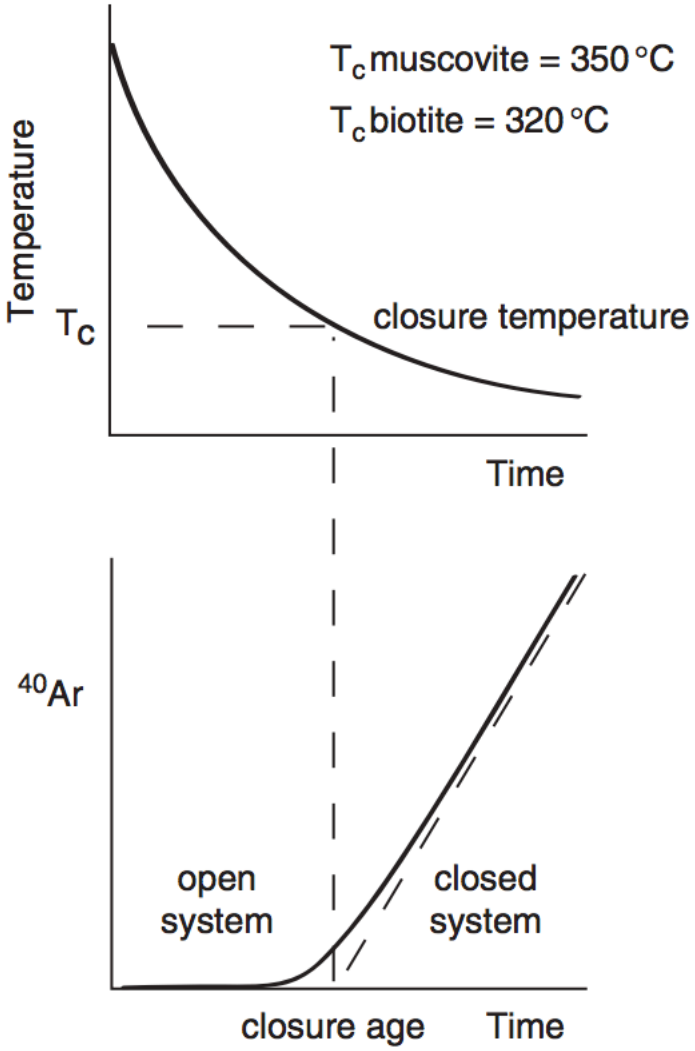

Figure 6.35 $^{40}Ar/^{39}Ar$ system. The system is open to diffusive loss of ^{40}Ar at high temperatures, becoming progressively more closed and retentive of ^{40}Ar as temperature cools during exhumation.

Closure temperature varies depending on what's escaping, and on what mineral it's escaping from.

(6) Fission track.

why are these not straight lines?

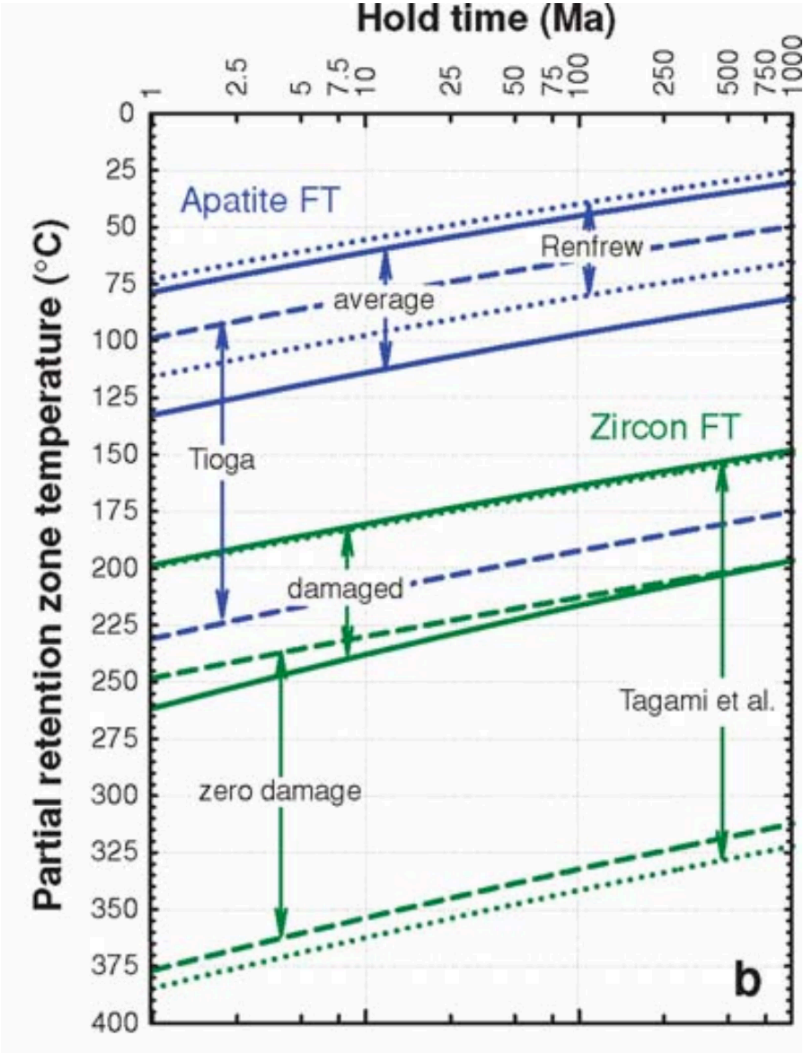

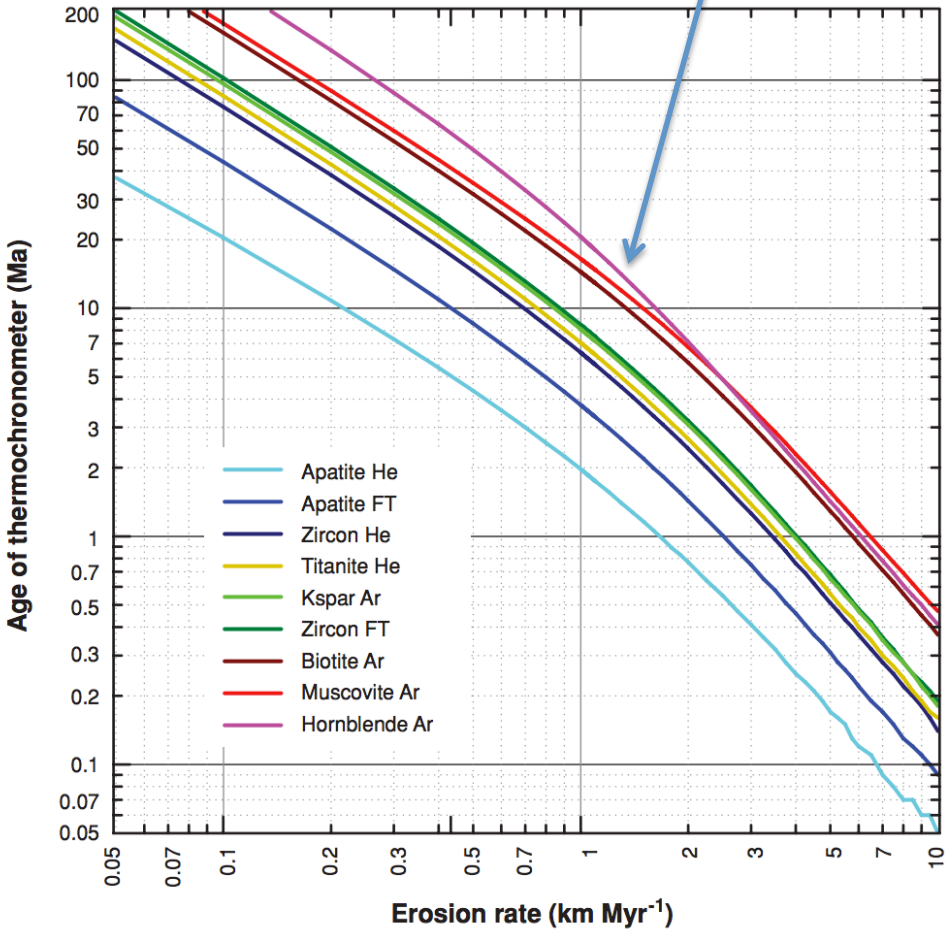

Mountain belt uplift:

Pe = L*u/kappa ~ 30 km*(1 mm/yr)/10^{-6} m^2s^{-1} ~ 1

Reiners & Brandon,
Annual Reviews 2006

Example application: Olympic Peninsula

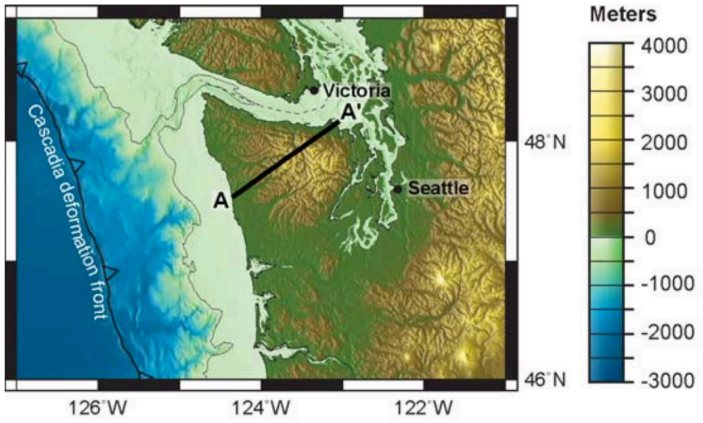

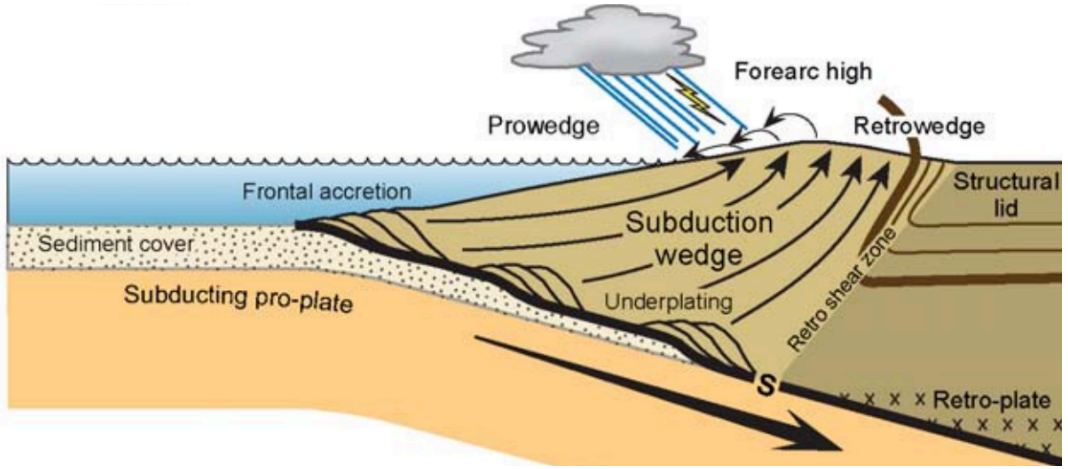

"strath" rates: uplift of dated marine terraces

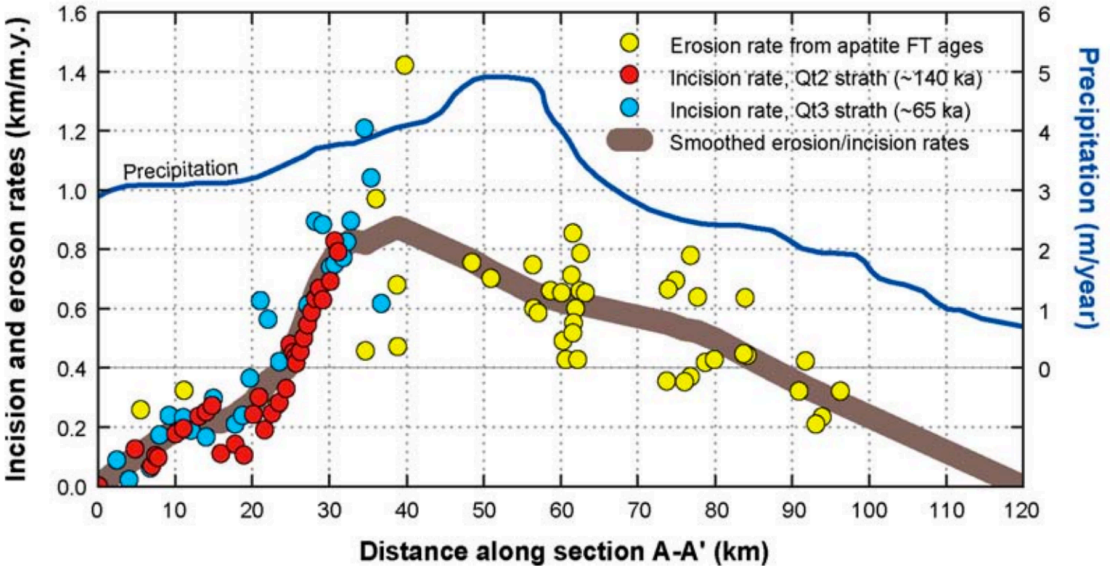

(7) (U-Th)/He & other exhumation methods.

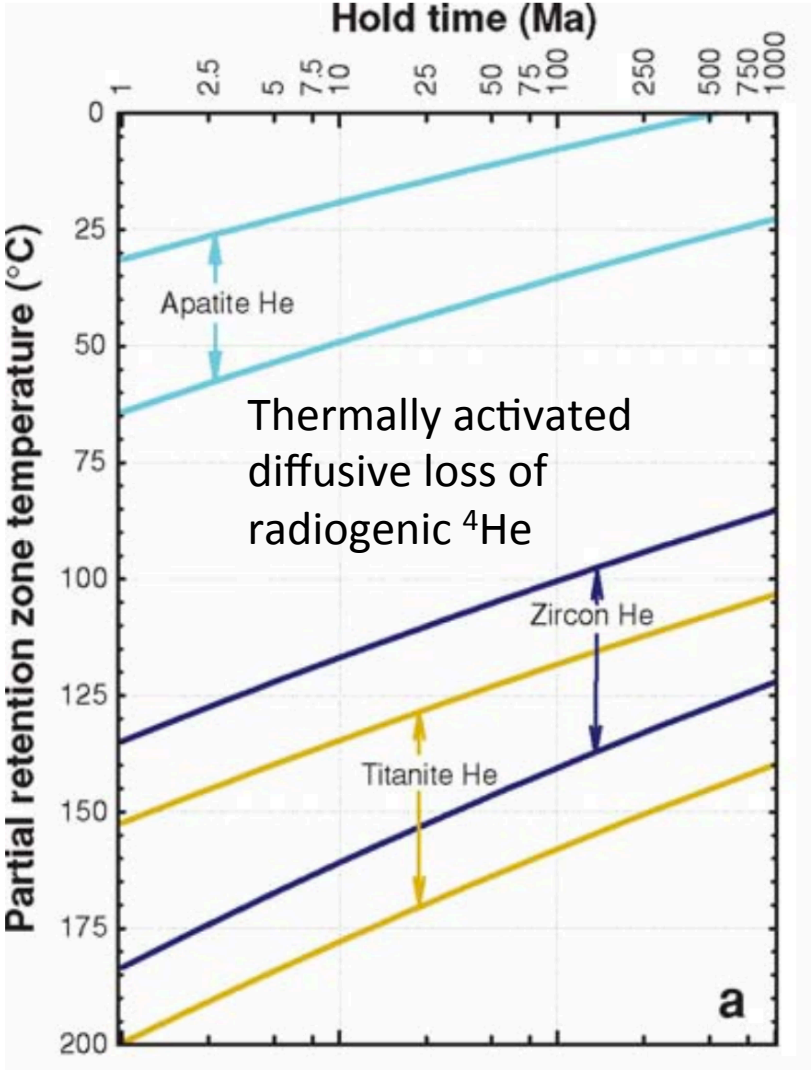

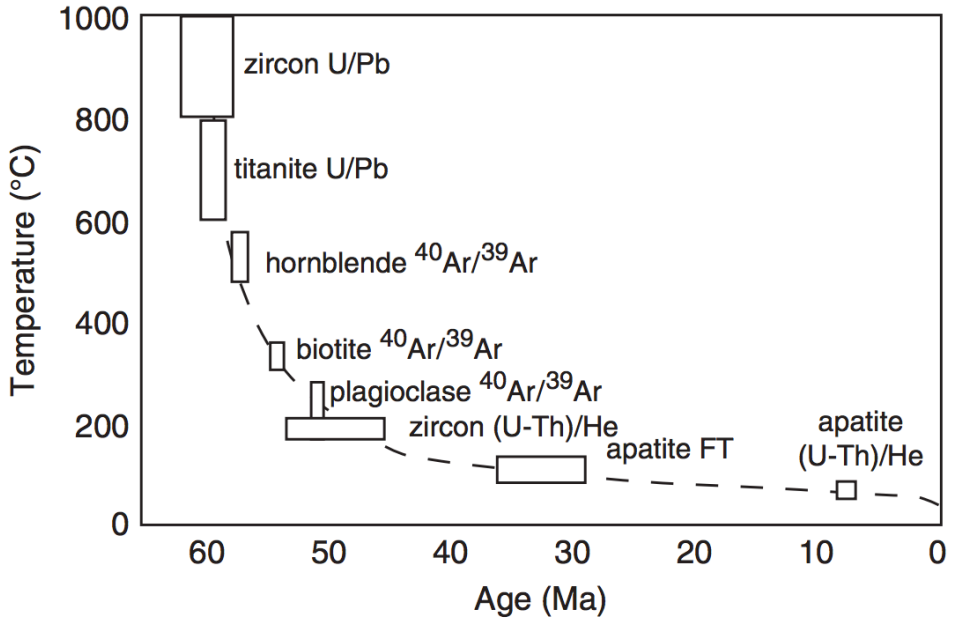

Figure 6.33 Temperature history of the Speel pluton, Alaska, derived from several thermochronometers. The data reveal rapid cooling after emplacement, followed by rapid cooling caused by exhumation after 10 Ma (after Reiners, 2005, Figure 3A and references therein, with permission from the American Geophysical Union).

(7) - Detrital thermochronology

Enabling technology: $^{40}Ar/^{39}Ar$ ages of individual grains

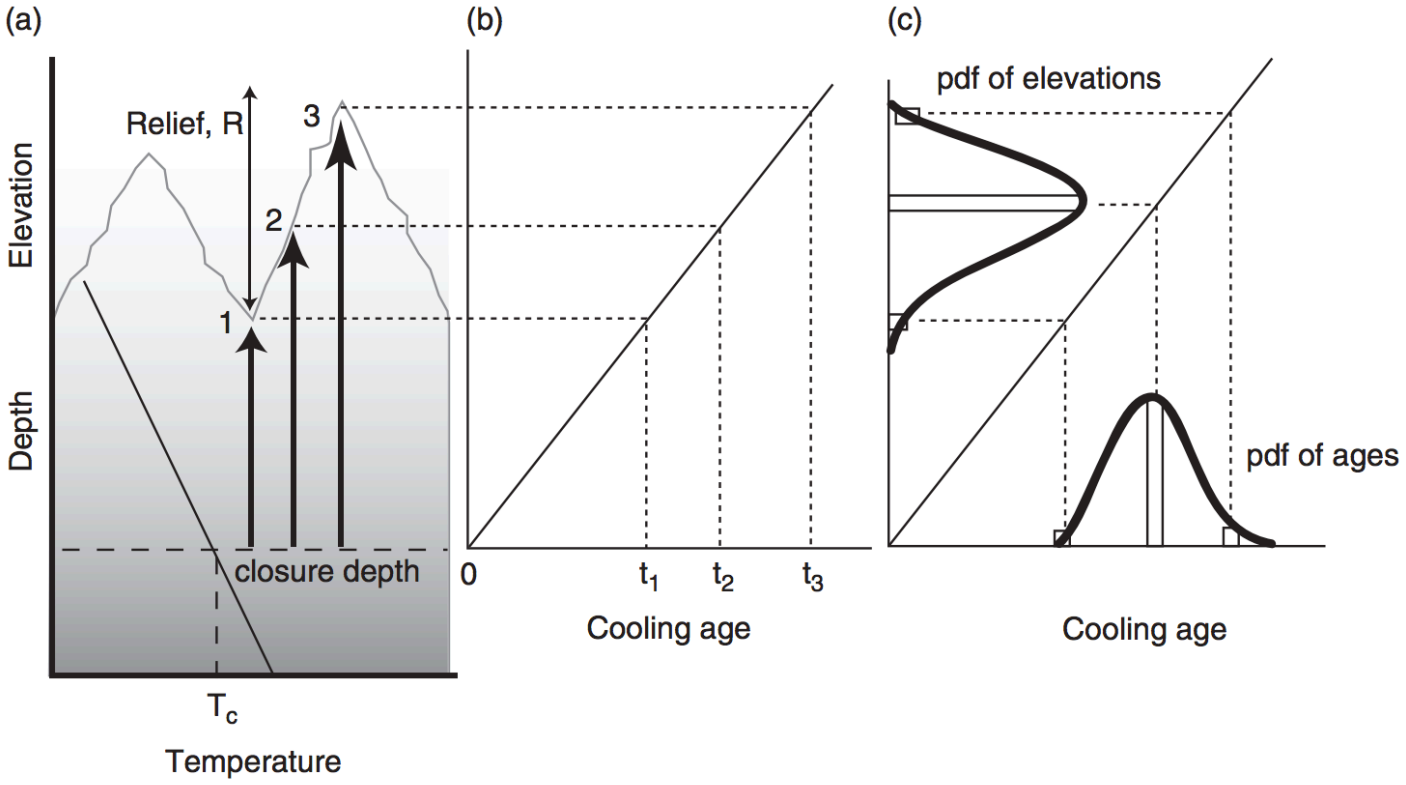

Figure 6.36 (a) Use of elevation profiles to infer exhumation rate in a steady-state landscape. (b) Expected age-elevation distribution in a uniformly eroding landscape such that the rate of erosion in the valley bottom is identical to that at the crest of the mountain. The long-term erosion rate can then be determined to be $R/\Delta t$, where Δt is the difference between ages at the mountain crest and valley trough. (c) The detrital method in which the pdf of ages from a sediment sample in a stream draining this landscape is interpreted in the light of the pdf of elevations in the catchment (its hypsometry). In a uniformly eroding landscape and steadily eroding landscape the pdf of elevations should map directly onto the pdf of cooling ages. Note that the interpretation of the cooling ages depends upon one's assumption about the geothermal gradient, which dictates the assumed cooling depth (after Brewer *et al.*, 2003, Figure 2, with permission from Blackwell Publishing).

(8) Shared event of known age.

Berlin et al. JGR-Earth Surface, 2007

Example: Roan Plateau, NW Colorado:

8 Ma incision
by Colorado River

Test of streampower incision model

See also Crosby & Whipple JGR 2006.

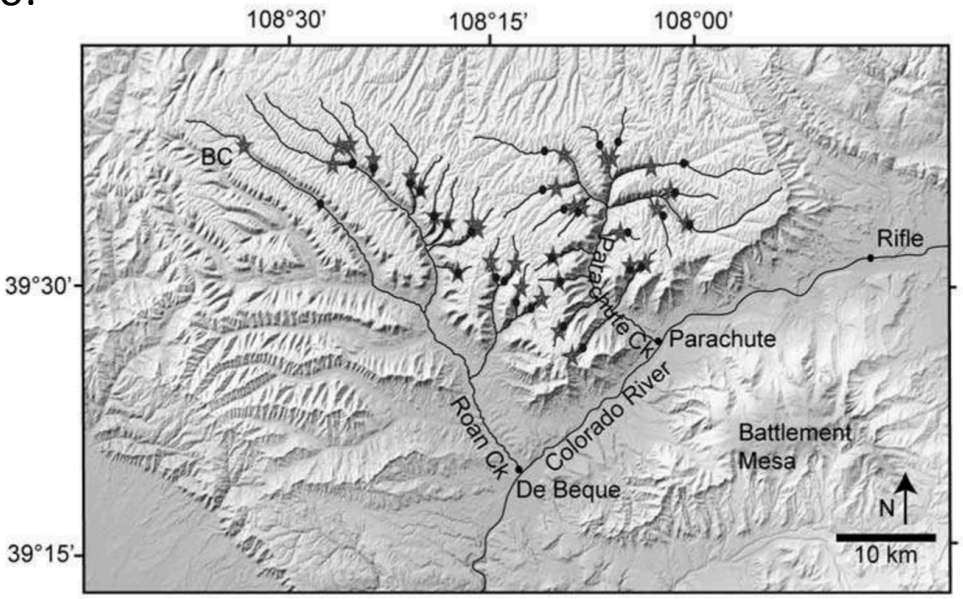

Figure 8. Modeled and observed knickpoint locations on the Roan Plateau. Solid circles indicate the modeled knickpoint positions and stars indicate observed knickpoint locations obtained from DEM analysis. BC–Brush Creek.

Strengths: Natural experiment.
Weaknesses: Relative, not absolute method (though can be calibrated by other methods)
Age range of applicability: Unrestricted in principle; in practice, post-180 Ma
(for which ~complete plate reconstructions are available).

Gondwana rifting

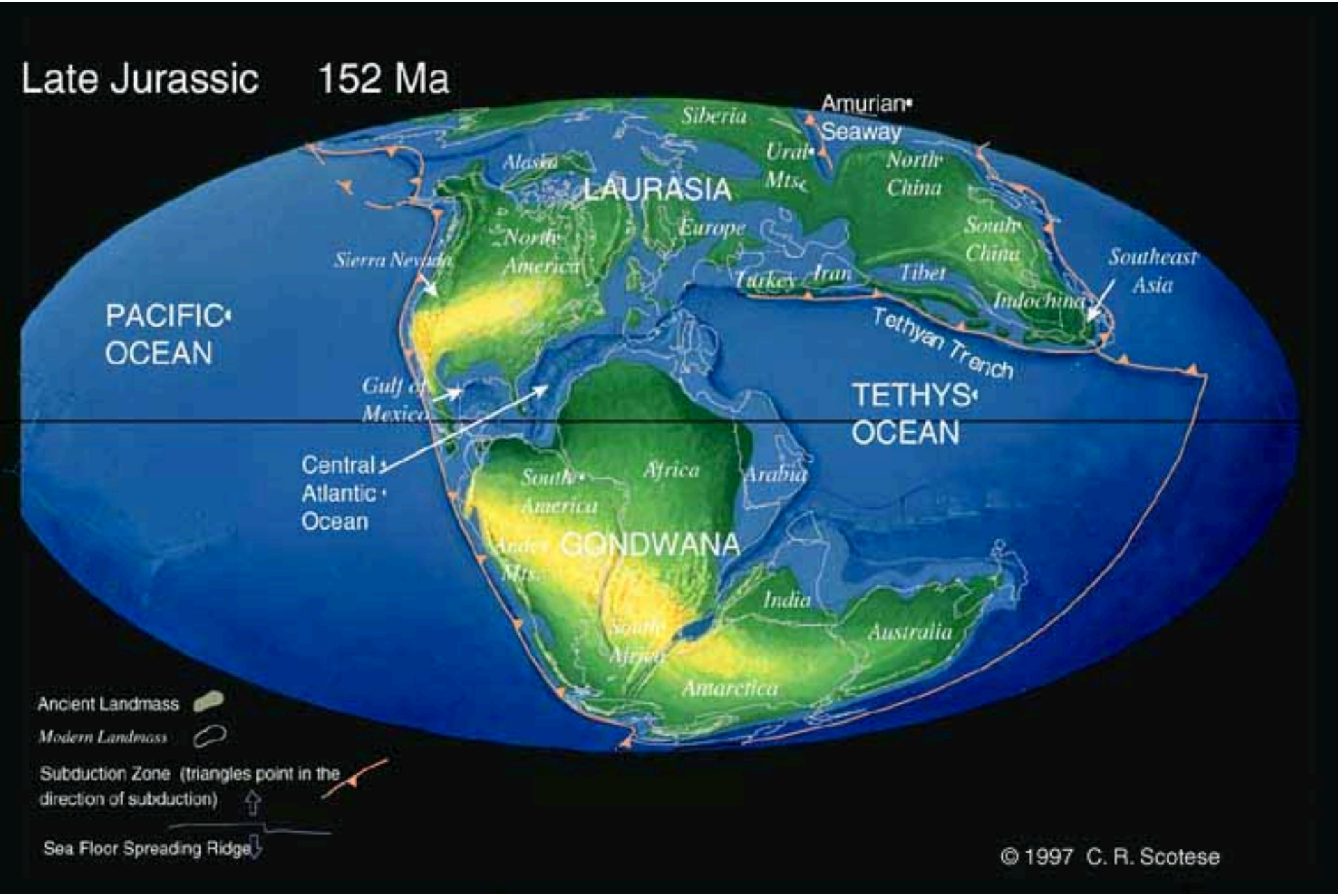

(8) Shared event of known age

Other example: Gondwana Scarp,
known as “Great Escarpment” in S. Africa

South Africa: rifting ~160 Ma
(plate tectonic reconstruction)
Scarp retreat rate: ~1 km/Myr

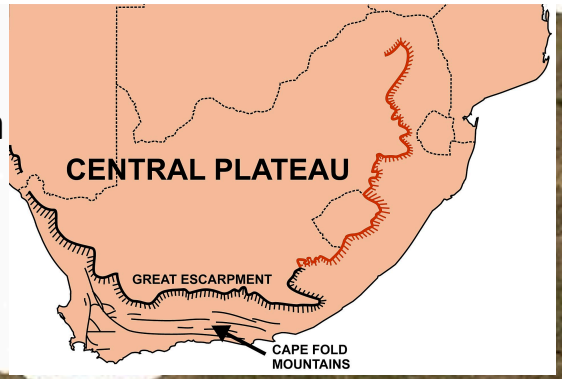

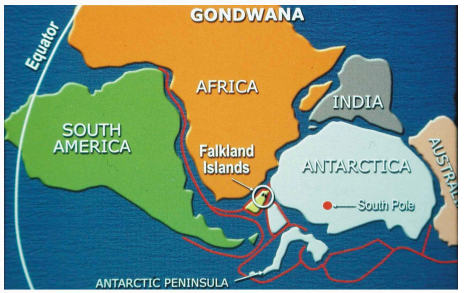

Gondwanaland reconstruction c.400 million years ago

Scarp retreat following continental break-up is constrained by apatite fission-track data

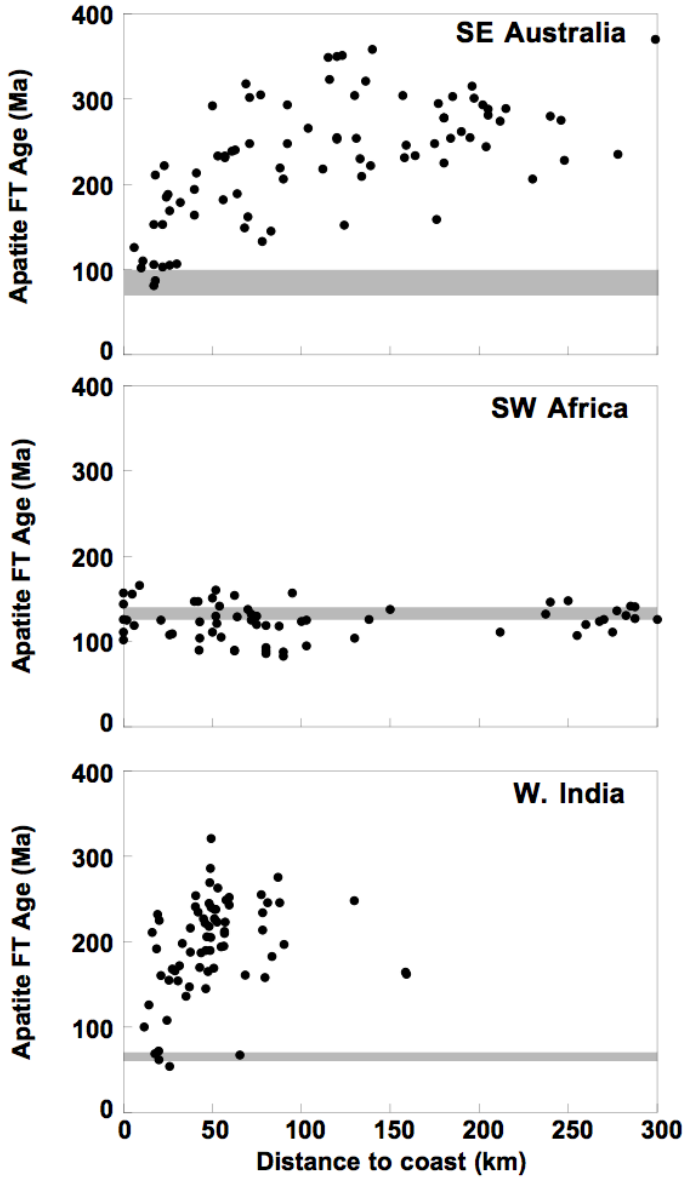

(9) The sedimentary record.

method with great promise for the future; see required reading Allen 2008

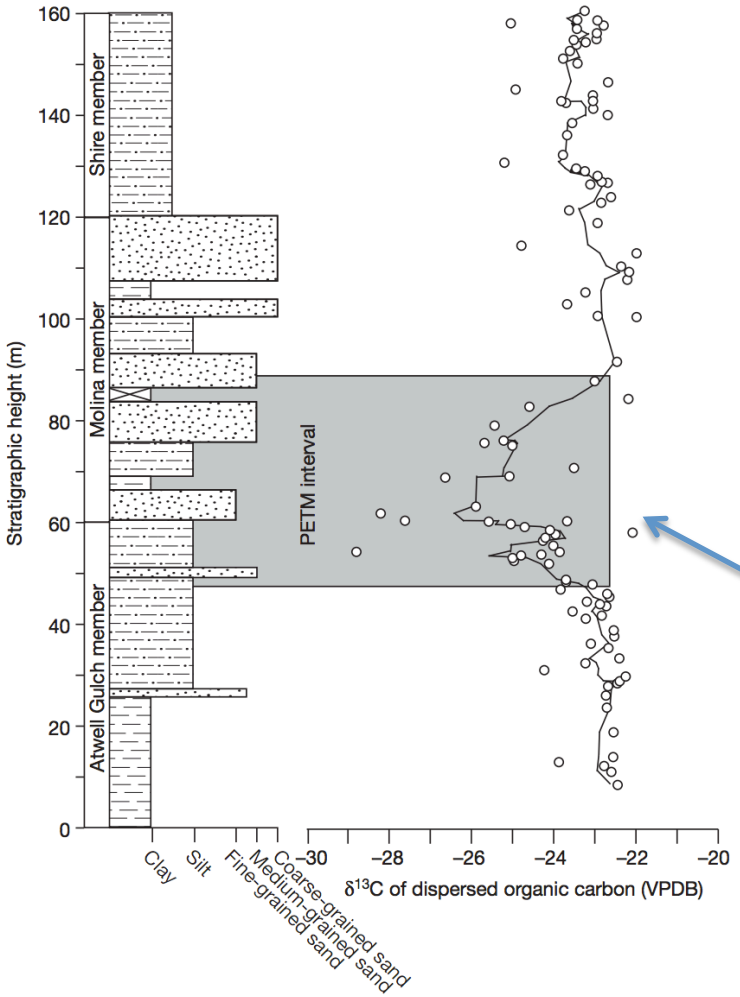

Foreman et al. Nature 2012

4-6 deg C increase in global T accompanied by 2x-4x increase in pCO_2

Strengths: Records information about fully-vanished landscapes.
Weaknesses: Changes in grain size + channel dimensions have multiple possible explanations.
Age range of application: < 3.5 Ga on Earth; <4.1 Ga on Mars (for orbiter methods)

Example (idealized model):

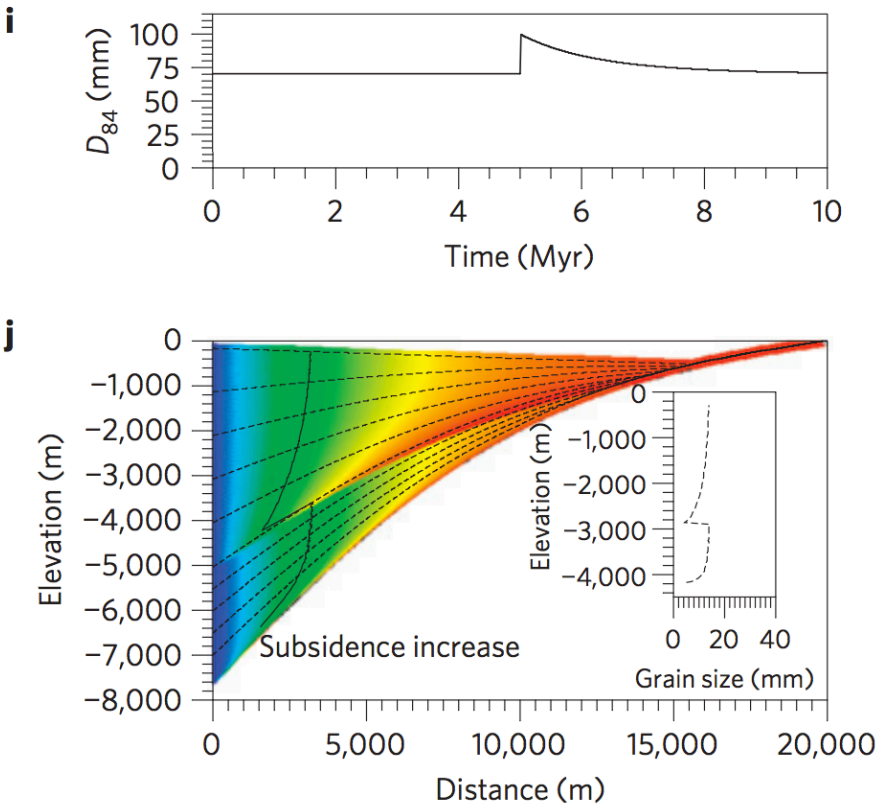

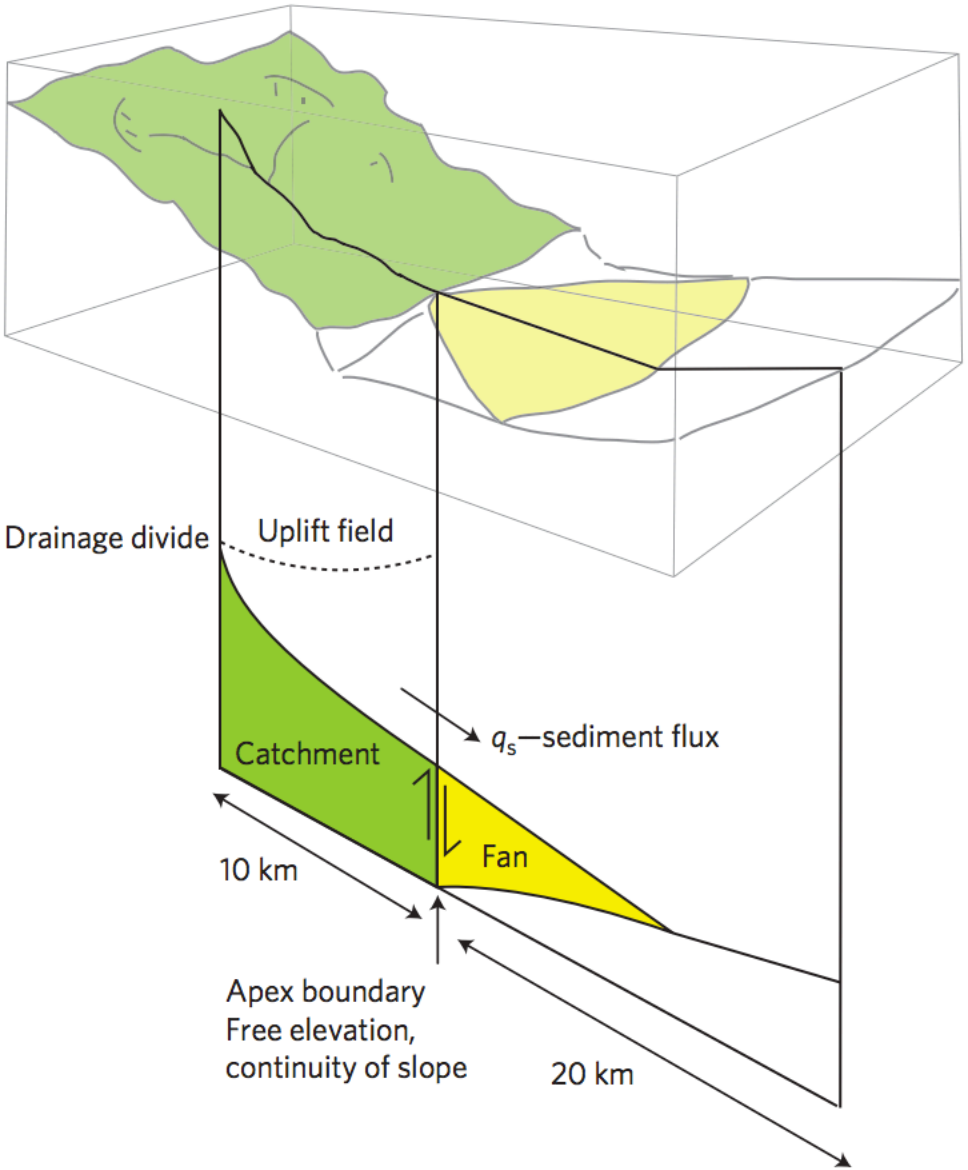

Figure 1 | Diagram of model domain. The uplifting catchment (green) is bounded by a vertical normal fault. The fault marks the transition from catchment to fan (yellow). In this idealized model domain, we maintain a continuity of slope and elevation across the apex[15,29].

Armitage et al. Nature Geoscience 2011

Integration and cross-checking of methods.

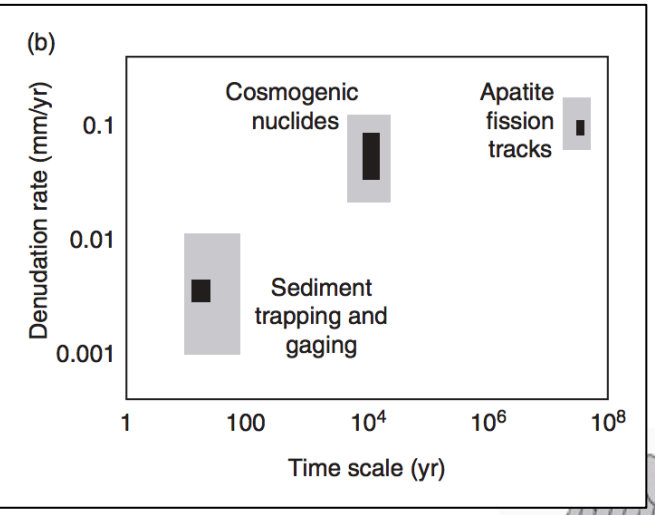

Anderson & Anderson, ch. 6

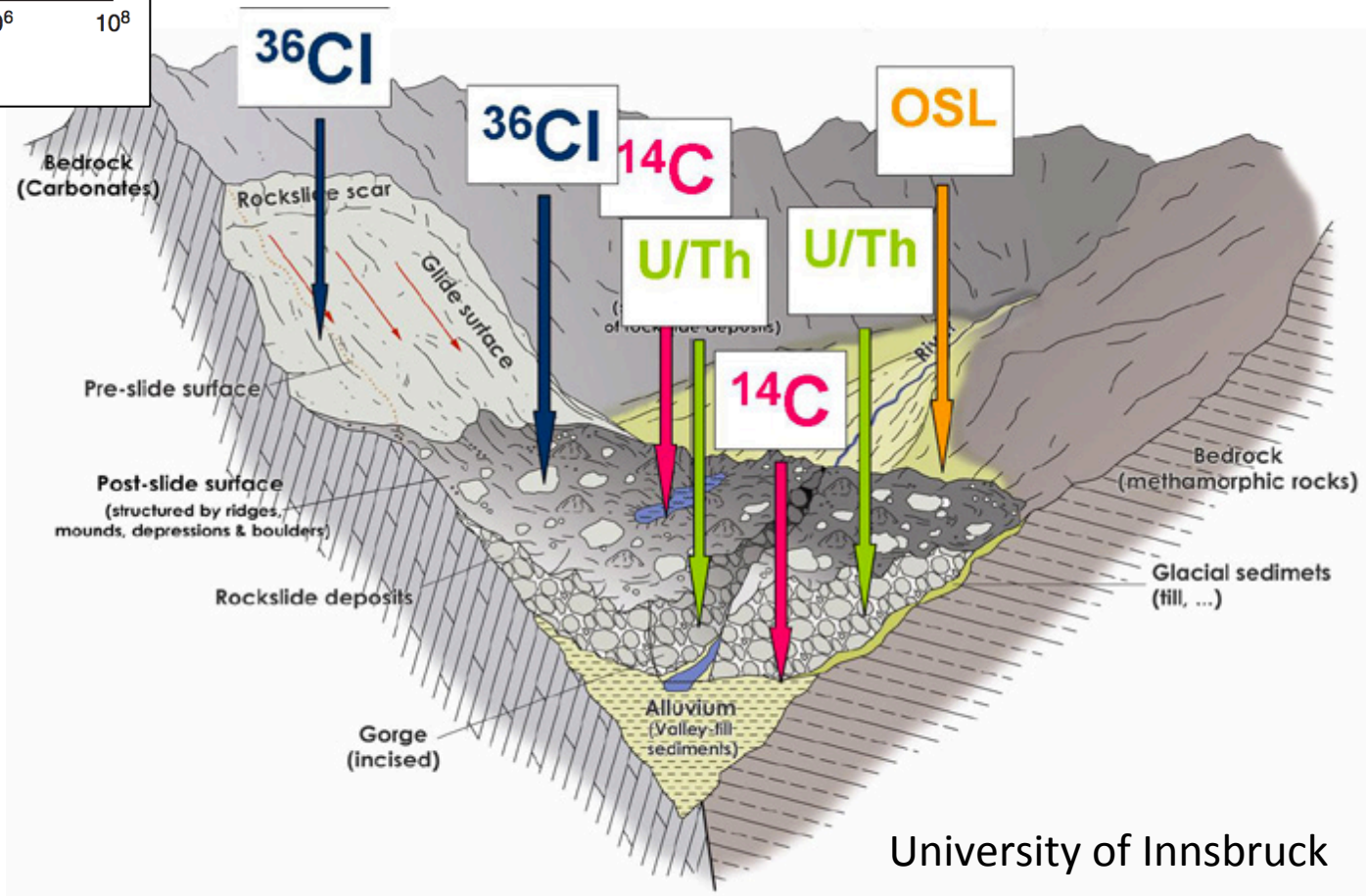

University of Innsbruck

Landscape evolution: sources of data

SOME MAJOR LANDSCAPE EVOLUTION PROBLEMS

DATE/RATE DATA ON EARTH

DATE/RATE DATA ON OTHER PLANETS

(P1) Crater-density constraints on burial and exhumation.

CONCEPT:

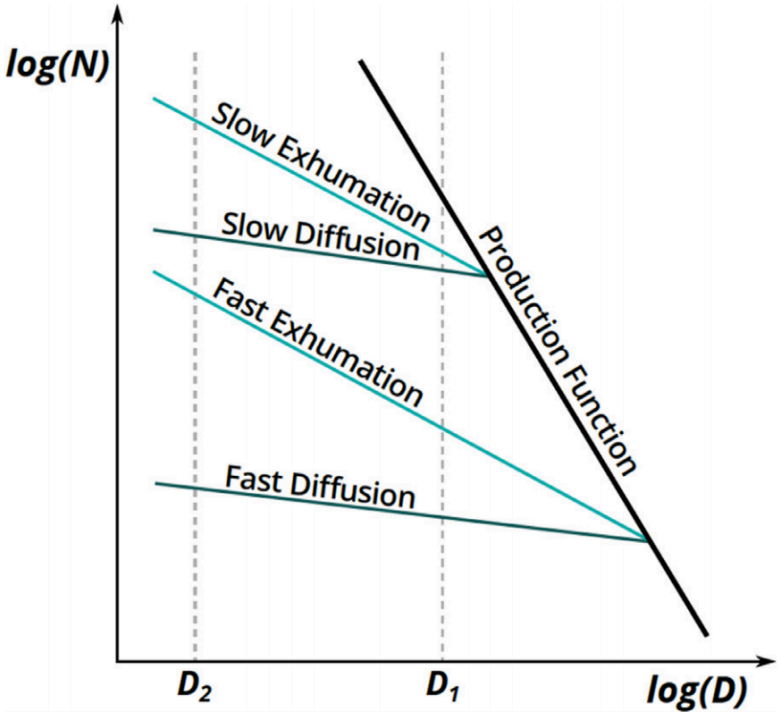

DATA:

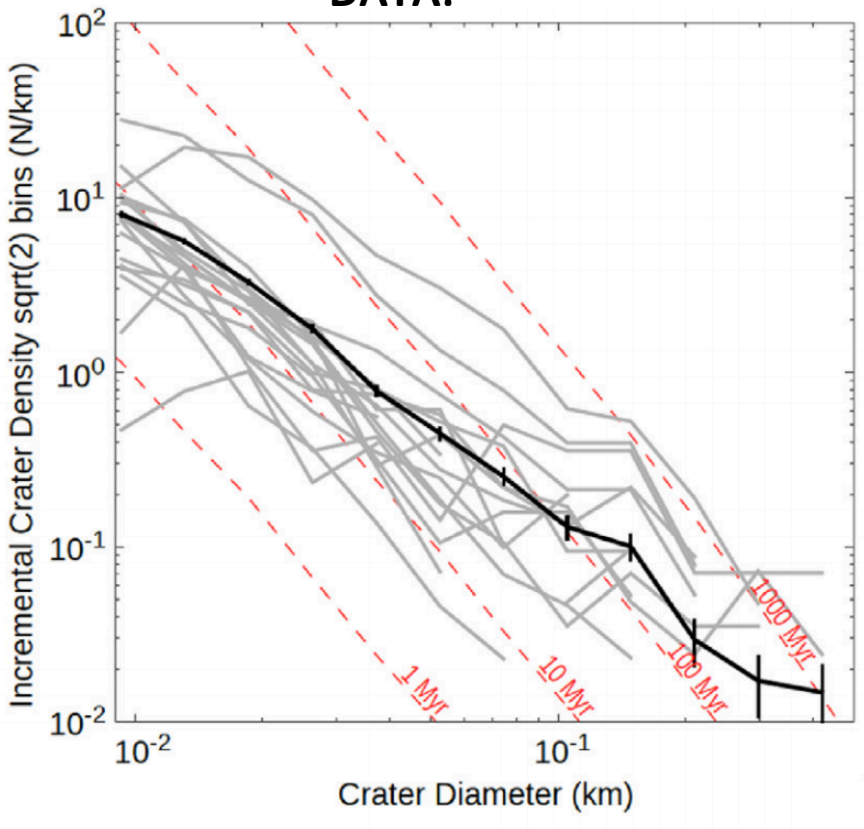

Kite & Mayer 2017

Strengths: Can be applied anywhere on Mars;
Can give past sedimentation rates.

Weaknesses: Difficult to date steep slopes (small area, distorted craters)

Age range of validity: In principle, applies to all timescales.
In practice, restricted to 1-100 Myr for erosion rates

(P2) Statistical approaches (e.g. crater modification)

Fassett & Thomson, JGR-Planets, 2014 – Goal:measure crater degradation on the moon vs. time. Plot the diffusional degradation of individual craters as a function of the crater density of the terrains that host them. Map the crater density to absolute age using Apollo radiometric dates.

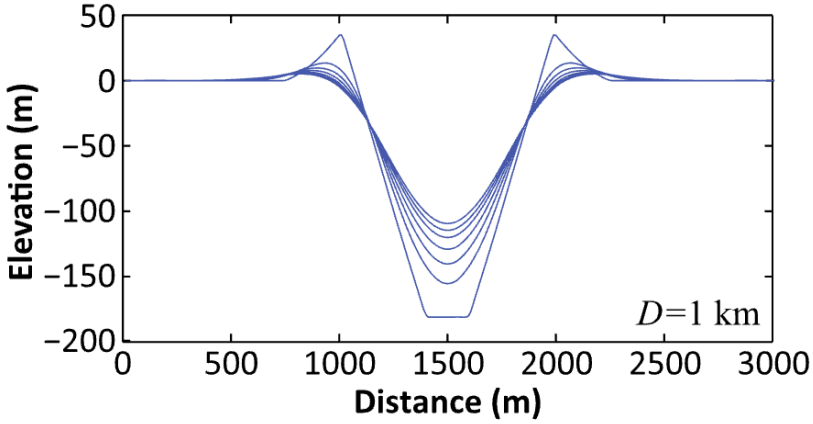

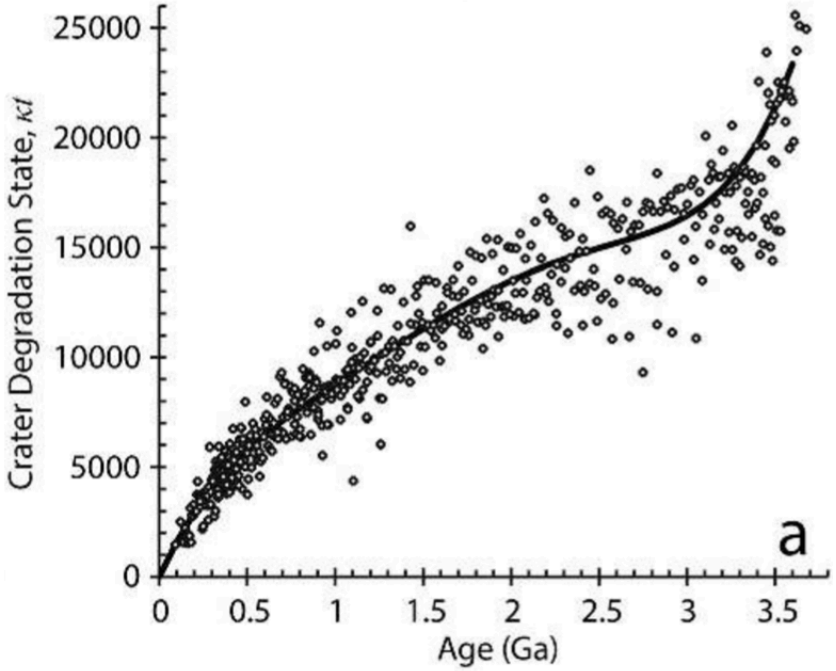

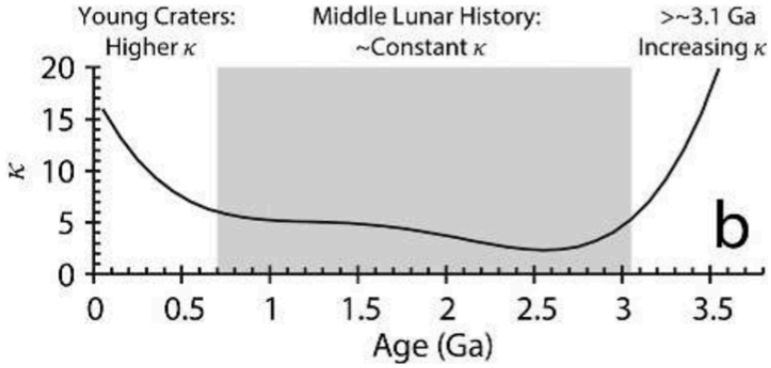

Key points

- For each Earth-based dating method, know the principle, advantages, disadvantages, example application, age range of application, for each technique.
- Explain the evidence for and against a Pleistocene uptick in global erosion on Earth (two arguments for and two arguments against, plus geographic context)

Natural environmental radiation causes charge (electrons and holes) to become trapped when grains are buried in the ground, as bonding electrons are excited from their valence positions, and a small fraction become trapped within the crystal lattice (**Figure 2**). Electron and hole traps are formed at point defects such as those formed by elemental substitution, for example, where Ti replaces Si in quartz. Charge may be compensated by the presence of alkali ions, for example, species such as an electron trap $[TiO_4/Li^+]^\circ$, or the hole center $[AlO_4]^\circ$, known from electron paramagnetic resonance studies (e.g., Weil 1984). Although several models have been proposed (e.g., Itoh et al. 2002), the detailed structure of the OSL electron traps in quartz continues to be explored; the Al hole center mentioned above is likely responsible for the quartz OSL emission in the UV region around 360–380 nm (Martini et al. 2009).

Backup slides

Transient hillslope evolution

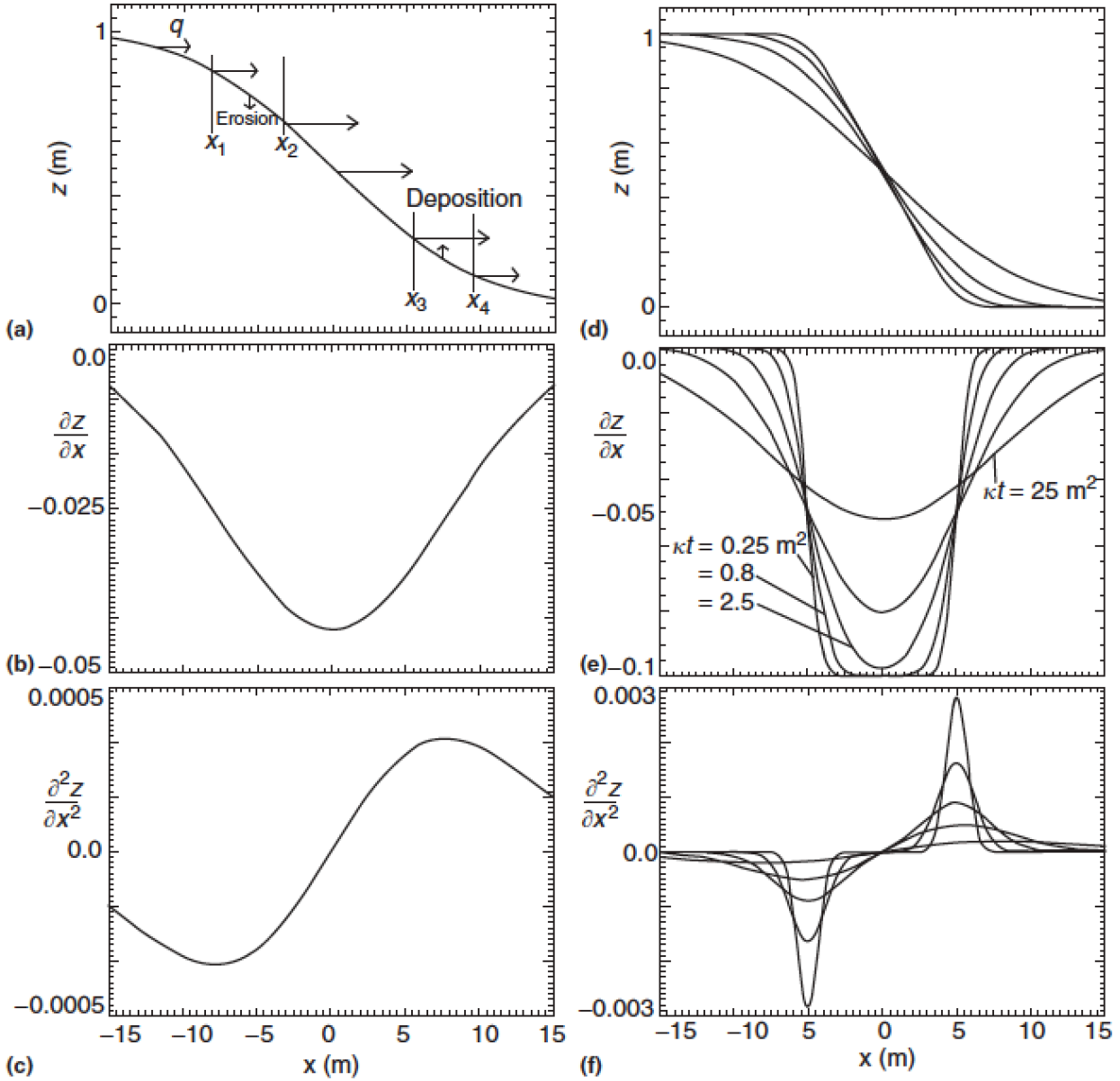

Figure 2 Evolution of a topographic scarp, illustrating (a) elevation, (b) slope, and (c) curvature. In (a), arrows of varying length represent the sediment flux at each point. In the diffusion model, the flux is proportional to the local slope, and the resulting raising or lowering rate of the surface is proportional to the change in flux per unit length, which, in turn, is proportional to the curvature. (d)–(f) Graphs of elevation, slope, and curvature for 5 times following scarp offset (κt=0.25, 0.8, 2.5, 8, and 25 m^2). Modified with permission from Pelletier, J.D., 2008. Quantitative Modeling of Earth Surface Processes. Cambridge University Press, Cambridge.

Pelletier, 2008, ch. 2; also Pelletier, 2013